Continental Shelf Research 298 (2026) 105632

Contents lists available at ScienceDirect

Continental Shelf Research

journal homepage: www.elsevier.com/locate/csr

Rates and pathways of organic matter remineralisation in different sedimentary environments of the Helgoland Mud Area, North Sea

Daniel Müller [a,b,*], Bo Liu [a], Moritz Holtappels [a,c], Walter Geibert [a], Susann Henkel [a,c], Sabine Kasten [a,b,c]

[a] Alfred Wegener Institute Helmholtz Centre for Polar and Marine Research, Am Handelshafen 12, 27570, Bremerhaven, Germany
[b] Faculty of Geosciences, University of Bremen, Klagenfurter Straße 2-4, 28359, Bremen, Germany
[c] MARUM—Center for Marine Environmental Sciences, University of Bremen, Leobener Straße 8, 28359, Bremen, Germany

A B S T R A C T

Coastal and shelf-sea sediments are hotspots for organic carbon (OC) remineralisation and burial. Using high-resolution solid-phase and pore-water data and diagenetic modelling, we investigated and quantified early diagenetic processes within sediments of the Helgoland Mud Area, SE German Bight. This included assessing the effects of bottom trawling and dumping of harbour sediments on rates and pathways of OC remineralisation. Our results show that aerobic respiration is the most important pathway of OC remineralisation, followed by sulphate reduction. Surprisingly, we observed no effect of different depositional and geochemical environments on the relative contribution of the different pathways of OC remineralisation in large parts of the study area, despite the wide range of mud contents, sedimentation rates, benthic OC fluxes and average reactivities of the OC reaching the sediment-water interface. This observation indicates that either (1) the variations within these parameters do not significantly influence the relative contribution of aerobic and anaerobic processes, or (2) the differences in these parameters are too insignificant to affect the contribution of the pathways. Exceptions are intensive bottom trawling, resulting in a lower contribution of aerobic respiration, enhanced sulphate reduction and higher overall OC remineralisation, and dumping of harbour sediments showing 7 to 12 times lower OC contents compared to harbour sediments and hence low OC remineralisation rates. This indicates a significant impact of benthic and pelagic remineralisation and ultimately CO_2 formation during dredging and dumping of harbour sediments.

1. Introduction

Marine sediments, in particular in coastal, estuarine and continental shelf areas, are the most important long-term carbon sinks on our planet (e.g., Hedges and Keil, 1995; Berner, 1982; Burdige, 2007; Lee et al., 2019). Continental shelf sediments are known to store organic carbon (OC) on geological timescales, and thus, sedimentation represents one of the key natural processes removing particulate organic carbon from the rapidly cycling and heavily anthropogenically influenced carbon pools of the ocean and atmosphere (e.g., Burdige, 2007). However, before reaching the sediments, large parts of the OC are remineralised on short time scales within the water and only a small proportion is deposited on the seafloor, depending on its origin and reactivity, along with water depth and the settling velocity of particles and aggregates (e.g., Suess, 1980; Berner, 1982; Middelburg et al., 1997). The balance between the flux of OC to the seafloor and OC remineralisation within the sediments is decisive for the burial of OC and thus the ultimate release of CO_2 back into the fast-cycling carbon pools of the water column and the atmosphere (e.g., Canfield, 1994; Burdige, 2007). The long-term preservation of OC and thus the OC storage capacity of marine sediments is therefore controlled by the sedimentation rate and post-depositional aerobic and anaerobic remineralisation processes within marine sediments (e.g., Froelich et al., 1979; Berner, 1980; Canfield, 1994; Zonneveld et al., 2010).

The remineralisation of OC in marine sediments proceeds via a suite of electron-accepting processes, namely aerobic respiration, denitrification, manganese reduction, iron reduction, sulphate reduction and methanogenesis (Froelich et al., 1979). Among these different remineralisation pathways, aerobic degradation of OC is the most energy-yielding remineralisation process (e.g., Froelich et al., 1979; Jørgensen and Kasten, 2006). Below the oxic zone, where oxygen is consumed by aerobic respiration, sulphate reduction has been shown to be the dominant anaerobic remineralisation pathway (e.g., Jørgensen, 1982, 2021; Middelburg et al., 1993; Jørgensen and Kasten, 2006; Bowles et al., 2014) and its magnitude is controlled by benthic OC flux on a global scale (Jørgensen, 2021 and references therein). However, the other pathways can also make a major contribution to overall remineralisation in continental margin and shelf sediments (e.g., Canfield

* Corresponding author. Alfred Wegener Institute Helmholtz Centre for Polar and Marine Research, Am Handelshafen 12, 27570, Bremerhaven, Germany
E-mail address: daniel.mueller@awi.de (D. Müller).

https://doi.org/10.1016/j.csr.2025.105632
Received 27 July 2025; Received in revised form 28 November 2025; Accepted 23 December 2025
Available online 1 January 2026

et al., 1993a; Thamdrup and Canfield, 1996). Anaerobic processes are of particular importance in coastal and shelf sediments, as oxygen is rapidly consumed in the uppermost millimetres to centimetres of the sediments (e.g., Canfield et al., 1993a). Anthropogenic activities in coastal and shelf seas, like bottom trawling, sediment dredging and dumping as well as the construction and use of offshore infrastructures, have been shown to significantly impact the OC cycle in cohesive sediments, reducing their natural OC storage capacity by increasing the remineralisation of OC and influencing the redox pathways of OC degradation (e.g., van de Velde et al., 2018; Paradis et al., 2021; De Borger et al., 2021b; Clare et al., 2023; Heinatz and Scheffold, 2023; Zhang et al., 2024; Porz et al., 2025).

On the North Sea shelf, sedimentation is limited to only a few regions, with the most important depocentres for fine-grained and organic-rich sediments within the German Bight of the North Sea being the Helgoland Mud Area (HMA), together with the Wadden Sea mudflats and estuaries (Figge, 1981; Bockelmann et al., 2018; Chen et al., 2025). In previous studies, Müller et al. (2025) and Wei et al. (2025) evaluated how the different depositional and geochemical conditions control the preservation and burial of OC in the sediments of the HMA using high spatial resolution pore-water and solid-phase datasets. Sedimentation rate and the reactivity/origin of particulate organic matter were shown to be the most important factors for efficient preservation of organic carbon in the sediments. This combination of depositional characteristics in the sediments of the HMA results in high OC burial rates of 57.3 gC m^{-2} yr^{-1} and burial efficiencies of up to 78 % for respective sedimentation rates of 4.5 mm yr^{-1}. The sites at which sediments show these high OC burial rates and efficiencies are located proximal to the outflows of the rivers Elbe and Weser. For the entire HMA, the calculated OC burial fluxes result in a total annual organic carbon accumulation of 0.011 Tg C yr^{-1}. These results highlight the importance of depocentres for fine-grained sediments as important natural carbon sinks: compared to the North Sea shelf average, the HMA accumulates 8.4 times more OC (Müller et al., 2025). In addition to differences in depositional conditions, Müller et al. (2025) reported non-steady state pore-water conditions at four shallow-water sites in the eastern part of the HMA, most likely due to previous storm events.

In this study, we aim to explore how the different depositional and geochemical conditions prevailing in the HMA affect the rates and pathways of OC remineralisation. We build on the dataset by Müller et al. (2025) and include further pore-water concentration data describing all relevant reactants and products of biogeochemical processes. Using this comprehensive data set, we apply a full diagenetic model considering both steady-state and non-steady-state conditions at individual sites. The objectives are (1) to quantify the rates and metabolic pathways of both aerobic and anaerobic OC degradation in the surface sediments of the HMA, including the impact that transient states caused by storm-induced pore-water mixing have on the determination of the rates of different metabolic pathways, (2) to identify the controls of the different depositional and geochemical environments in the HMA on the rates and metabolic pathways of OC degradation and (3) to evaluate the impact of anthropogenic activities in areas of intense bottom trawling and of dumping of harbour sediments on total rates and metabolic pathways of OC remineralisation.

2. Study area

The southeastern part of the North Sea Shelf shows water depths ranging between 10 and 40 m and is dominated by the presence of unconsolidated sediment of primarily glacial, pro-glacial and fluvial sources (von Haugwitz et al., 1988; de Haas et al., 2002; Sievers et al., 2021). The area was submerged during the mid-Holocene by the transgressive North Sea, following the relative sea-level low-stand of the Last Glacial Maximum, and marine depositional processes thus have only occurred over the last ~8000 years (e.g., Vink et al., 2007). Lateral transport and deposition-resuspension cycles of material are characteristic seafloor processes in sand-dominated sedimentary environments (Figge, 1981; de Haas et al., 1996, 2002; Zeiler et al., 2000). Strong hydrodynamic conditions limit sedimentation to only a few regions, with the most important depocentres for fine-grained sediments in the German Bight of the North Sea shelf being the HMA together with the tidal flats of the Wadden Sea and estuaries (Figge, 1981). The HMA covers an area of approximately 500 km^2 (after von Haugwitz et al., 1988; Doll, 2015) and is located southeast of the island of Helgoland at water depths between 10 and 30 m below mean sea level (Fig. 1). The sediments originate from suspended particulate matter (SPM) of riverine input mainly from the Elbe and Weser rivers, primary production and local sediment redeposition (e.g., Puls et al., 1999; Wei et al., 2025). Coarse-grained layers are usually related to storm events (e.g., Gadow, 1969).

While bottom trawling activity is estimated to be generally low or absent in most parts of the HMA, the northwest of the HMA is significantly affected by it, with a swept area ratio ranging between 5 and 15 yr^{-1} (Hintzen et al., 2012; Eigaard et al., 2017; Thünen Institute, 2018) and highest modelled sediment mixing rates of 8.4 cm^3 cm^{-2} yr^{-1} (Müller et al., 2025). However, centuries of continuous bottom trawling in the German Bight and the North Sea (de Groot, 1984) could contribute significantly to the redistribution of sediments on the North Sea shelf. Further direct anthropogenic impacts on the sediments in the study area include the dumping of sediments at site Tonne E3, located at the western rim of the HMA. Here, harbour sediment, which is regularly dredged from the Elbe estuary and the Hamburg harbour, is dumped (e.g., Hamburg Port Authority, 2017). From the start of the sediment dumping at Tonne E3 in 2005 until June 2016, around 10.1 mio. m^3 were dumped, and from 2016 to 2022, annually between 1 and 1.5 mio. tons of dry substance were deposited at Tonne E3 (Hamburg Port Authority, 2020, 2024).

3. Material and methods

Sediment and pore-water samples were collected during RV Heincke expedition HE595 in March and April 2022 as part of the MARE:N "Oceans under Stress" collaborative project "Anthropogenic impacts on particulate organic carbon cycling in the North Sea" (APOC) funded by the German Ministry of Research and Education (BMBF). In this study, we present data from 14 sites at water depths between 11 and 31 m, well distributed over the entire Helgoland Mud Area (HMA) in order to cover the different depositional environments. Samples were retrieved using a multiple corer (MUC), which allowed sampling and investigating undisturbed sediment surface and subsurface (core lengths: 18–36 cm, Table 1). From each MUC deployment, two cores were used: one for pore-water sampling, and the second to determine pore-water oxygen concentrations by means of micro-oxygen-optodes and for subsequent sediment sampling. The geographical locations of the sampling stations within the HMA are reflected by site names, which indicate their relative position in the HMA (Fig. 1, Table 1).

Pore-water and sediment samples were taken in 1 cm intervals in the uppermost 10 cm and every second centimetre below. Pore water was extracted using rhizon samplers with an average pore size of 0.1 µm (Seeberg-Elverfeldt et al., 2005). Any potential oxidation and dilution of the pore-water samples by the MilliQ soaked rhizons were prevented by discarding the first extracted millilitre. Pore-water samples for nitrate (NO_3^-) and ammonia (NH_4^+) measurements were stored at −20 °C, and samples for sulphate (SO_4^{2-}) analysis at 4 °C, respectively. For hydrogen sulphide measurement, 1.5 ml of pore water was mixed with 0.6 ml oxygen-free zinc acetate solution and stored at 4 °C. Here and in the following, hydrogen sulphide comprises the sum of the dissolved sulphide species and is referred to as H_2S. Pore-water aliquots of 1 ml were acidified with 25 µl double-distilled concentrated HCl and stored at 4 °C for dissolved iron (in the following referred to as Fe^{2+}, for consistency and comparability with the modelled element species, oxidation states have not been determined) and dissolved manganese (in the following

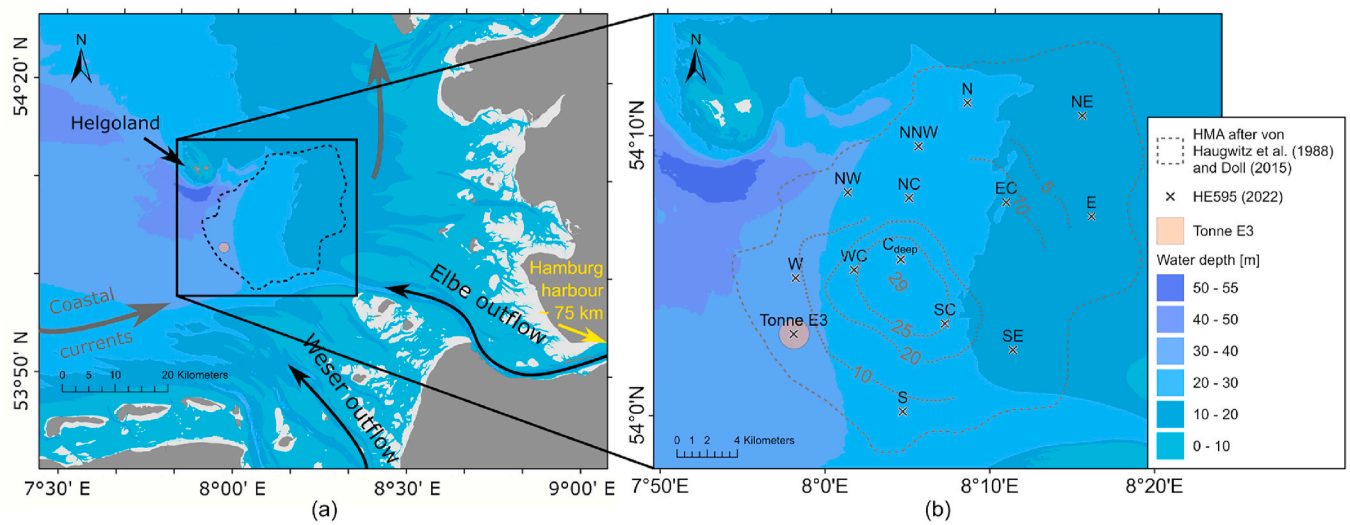

Fig. 1. (a) Overview of the Helgoland Mud Area (dashed line) after von Haugwitz et al. (1988) and Doll (2015) in the German Bight of the North Sea, coastal currents after Hertweck (1983; grey arrows) and the outflow of the Elbe and Weser river to the German Bight of the North Sea. The Hamburg harbour is ~75 km upstream of the Elbe river (southeast, indicated by the yellow arrow) (b) Locations and names of sampling sites (2022, black crosses) and location of the dumping site for harbour sludge Tonne E3 (orange dot, Hamburg Port Authority, 2017). Sediment thickness (dashed lines) after von Haugwitz et al. (1988). The maps were created using ArcGIS Pro (version 3.3). (For interpretation of the references to colour in this figure legend, the reader is referred to the Web version of this article.)

Table 1
Site name, station number, sampling date, coordinates, water depths and lengths of all MUC cores investigated in this study. Two different cores from the same MUC deployment were used for pore-water (PW) and solid-phase (SP) analyses resulting in slightly different core lengths.

Site name	Station number	Date	Latitude (N)	Longitude (E)	Water depth (m)	Core length PW (cm)	Core length SP (cm)
N	HE595_70-1	27.03.2022	54.188915	8.1395	19	20	26
NNW	HE595_98-3	30.03.2022	54.162653	8.090378	19.1	18	22
NE	HE595_67-5	26.03.2022	54.182054	8.256311	13.5	22	22
NW	HE595_1-3	17.03.2022	54.134669	8.019095	26	32	22
NC	HE595_69-2	27.03.2022	54.131856	8.081416	20.3	28	30
EC	HE595_97-1	30.03.2022	54.129986	8.180103	16.1	28	26
E	HE595_26-1	22.03.2022	54.122143	8.266746	11.3	24	22
W	HE595_12-3	20.03.2022	54.08331	7.967387	27.3	32	28
WC	HE595_6-1	18.03.2022	54.088596	8.026592	25.6	26	18
C_{deep}	HE595_9-1	19.03.2022	54.095192	8.073844	20	24	20
SC	HE595_45-1	24.03.2022	54.057359	8.119441	16.5	32	30
SE	HE595_41-4	23.03.2022	54.042098	8.188585	12	32	26
S	HE595_48-3	25.03.2022	54.004668	8.077746	21.8	28	28
Tonne E3	HE595_22-1	21.03.2022	54.049901	7.966345	25.4	20	20

referred to as Mn^{2+}, for consistency and comparability with the modelled element species, oxidation states have not been determined) analysis. After cutting off the rim that was in contact with the MUC liner, sediment samples for the determination of porosity, total organic carbon (TOC) content and sedimentation rate (based on $^{210}Pb_{xs}$) were transferred into Whirl-Pak® bags and stored at 4 °C.

Porosity, sedimentation rate (based on $^{210}Pb_{xs}$), TOC, dissolved inorganic carbon (DIC) content and its stable carbon isotopic composition (δ^{13}C-DIC) as well as oxygen profiles were determined as part of the study by Müller et al. (2025), and detailed methodological descriptions can be found therein. Data from the dumping site for harbour sludge Tonne E3 located in the southwestern HMA was added to the previously published data.

3.1. Pore-water analyses

In addition to the dataset presented by Müller et al. (2025), this study includes nitrate (NO_3^-), ammonium (NH_4^+), concentrations of dissolved iron and manganese, sulphate (SO_4^{2-}), as well as hydrogen sulfide (H_2S). All analyses were performed in the laboratories at the Alfred Wegener Institute Helmholtz Centre for Polar and Marine Research (AWI) in Bremerhaven. NO_3^- and NH_4^+ concentrations were analysed using a QuAAtro Continuous Segmented Flow Analyser (Seal Analytical) for a concentration range of 0.2–6.6 µmol l^{-1} and 2.5–102 µmol l^{-1}, respectively. Samples exceeding this range were subsequently diluted, and on average, the relative deviation was <2 % for duplicate measurements of all samples. Fe^{2+} and Mn^{2+} were analysed using inductively coupled plasma optical emission spectrometry (iCAP™ 7400 ICP-OES Analysator, Thermo Scientific), and details on the measurement can be found in Zhou et al. (2023). For both, the limits of detection were <1 µmol l^{-1}. Ion chromatography (930 Compact IC Flex, Metrohm) was used to determine sulphate concentrations with an accuracy error of <2 % and a precision error of ~1 %. Hydrogen sulphide concentrations were measured spectrophotometrically following the methylene blue method after Cline (1969) using a DR2800 spectrophotometer (Hach Lange). The limit of quantification was 0.01 mmol l^{-1}.

3.2. Geochemical model setup and parameterisation

Müller et al. (2025) determined total remineralisation rates based on diffusive oxygen uptake (DOU) derived from measured oxygen concentration profiles. Here, we use a comprehensive pore-water and solid-phase dataset to implement a full diagenetic model to assess the rates and metabolic pathways of both aerobic and anaerobic OC

degradation in the surface sediments of the HMA.

The reactive transport model consists of 16 species and 16 reactions (Tables 2–4) and uses the advection-transport-reaction equations for dissolved (Eq. (1)) and solid species (Eq. (2)) according to the approach followed by Van Cappellen and Wang (1996) and Boudreau (1996a):

$$\varphi_i \frac{\partial C_{i,j}}{\partial t} = \frac{\partial}{\partial z}\left(\varphi_i\left(\frac{D_{i,j}}{\theta^2} + D_{b,i}\right)\frac{\partial C_{i,j}}{\partial z}\right) - \frac{\partial \varphi_i v_i C_{i,j}}{\partial z} + \alpha_i \varphi_i (C_{0,j} - C_{i,j}) + \varphi_i \sum R_{i,j} \quad (1)$$

$$(1-\varphi_i)\frac{\partial G_{i,j}}{\partial t} = \frac{\partial}{\partial z}\left(D_{b,i}(1-\varphi_i)\frac{\partial G_{i,j}}{\partial z}\right) - \frac{\partial (1-\varphi_i) w_i G_{i,j}}{\partial z} + (1-\varphi_i)\sum R_{i,j} \quad (2)$$

where t is time; z is sediment depth and i, j represent subscripts depicting depth and species-dependence, respectively; φ is the porosity; C, G are the species concentration (aqueous (O_2, NO_3^-, SO_4^{2-}, NH_4^+, Mn^{2+}, Fe^{2+}, H_2S, DI^{12}C, DI^{13}C) and solid species (TOC$_1$, TOC$_2$, TOC$_3$, $MnO_2, Fe(OH)_3, FeS$), respectively); $C_{0,j}$ is the concentration of species j in bottom water; D is the diffusion coefficient; θ^2 is the tortuosity ($\theta^2 = 1 - 2\ln\varphi$; Boudreau, 1996b); D_b is the bioturbation coefficient; α is the bioirrigation coefficient; v, w are the burial velocity of the aqueous and the solid phase, respectively; $\sum R_{i,j}$ is the sum of the reaction rates affecting the given species j. All the species, parameters and boundary conditions except those given in the text are listed in Table S1.

$$\text{Conversion factor}: f_c = \rho\frac{1-\varphi}{\varphi}$$

Porosity data showed no apparent decrease with depth at all stations and was therefore set to be constant. The burial velocity of the aqueous and solid phases was therefore equal to the sedimentation rate ($v = w = \omega$).

Bioturbation-induced mixing was assumed to follow a modified logistic function with the break attenuation depths (Mogollón et al., 2016; Volz et al., 2020):

$$D_b = D_b^0 \exp\left(\frac{z_{mix} - z}{z_{att}}\right) \Big/ \left(1 + \exp\left(\frac{z_{mix} - z}{z_{att}}\right)\right) \quad (3)$$

where D_b^0 is constant, representing the maximum bioturbation coefficients at the sediment-water interface (SWI); z_{mix} is the depth, where D_b^0 becomes half its value and z_{att} is the attenuation depth of the biogenically induced mixing. The bioirrigation coefficient α for the dissolved species is approximated as (Boudreau, 1997):

$$\alpha = \alpha_0 \exp(-z / z_{irr}) \quad (4)$$

where α_0 and z_{irr} describe the bioirrigation intensity at the SWI and its attenuation depth, respectively.

NH_4^+ in pore water undergoes rapid and reversible equilibrium adsorption on sediment. Following Berner (1980) and Burdige (2006), we implemented the effect of adsorption into the model as the following equation:

$$(1+K_N)\varphi_i\frac{\partial C_{NH4,i}}{\partial t} = \frac{\partial}{\partial z}\left(\varphi_i\left(\frac{D_i}{\theta^2} + D_{b,i}(1+K_N)\right)\frac{\partial C_{NH4,i}}{\partial z}\right)$$

$$-\frac{\partial (v_i + w_i K_N)\varphi_i C_{NH4,i}}{\partial z} + \alpha_i\varphi_i\left(C_{NH4,0} - C_{NH4,i}\right) + \varphi_i\sum R_i \quad (5)$$

where K_N is the dimensionless adsorption coefficient defined as a constant ($K_N = 1.4$) (Van Cappellen and Wang, 1996).

The primary and secondary redox reactions are listed in Table 2 and the rate expressions are given in Table 3. For TOC, the Redfield stoichiometry (C:N = 106:16) was assumed in the model. The organic matter degradation rate (R_{TOC}) is modelled by using a 3-G model to account for the heterogeneity of organic matter and its evolution during burial (Jørgensen, 1978). This model is based on the assumption that organic matter is composed of three discrete compound classes (labile C_{org}^1, metabolisable C_{org}^2 and refractory C_{org}^3), each characterised by a specific degradability σ_1, σ_2 and σ_3. The rate of organic matter degradation was calculated as $R_{TOC} = -\sum_{i=1}^{3}\sigma_i C_{org}^i$. The apparent reactivity

Table 2
Chemical reactions considered in the transport-reaction model.

Name	Reaction
Primary redox reaction	
Aerobic respiration (R_1)	$OM + (1+2a)O_2 \rightarrow CO_2 + aNO_3^- + aH^+ + (1+a)H_2O$
Denitrification (R_2)	$OM + \frac{4}{5}NO_3^- + \left(\frac{4}{5}+a\right)H^+ \rightarrow CO_2 + aNH_4^+ + \frac{2}{5}N_2 + \frac{7}{5}H_2O$
Manganese reduction (R_3)	$OM + 2MnO_2 + (4+a)H^+ \rightarrow CO_2 + aNH_4^+ + 2Mn^{2+} + 3H_2O$
Iron reduction (R_4)	$OM + 4Fe(OH)_3 + (8+a)H^+ \rightarrow CO_2 + aNH_4^+ + 4Fe^{2+} + 13H_2O$
Sulphate reduction (R_5)	$OM + \frac{1}{2}SO_4^{2-} + (1+a)H^+ \rightarrow CO_2 + aNH_4^+ + \frac{1}{2}H_2S + H_2O$
Re-oxidation reactions	
Nitrification (R_6)	$NH_4^+ + 2O_2 \rightarrow NO_3^- + H_2O + 2H^+$
Manganese oxidation (R_7)	$Mn^{2+} + \frac{1}{2}O_2 + H_2O \rightarrow MnO_2 + 2H^+$
Iron oxidation (R_8)	$Fe^{2+} + \frac{1}{4}O_2 + \frac{5}{2}H_2O \rightarrow Fe(OH)_3 + 2H^+$
Manganese oxidation by $\boldsymbol{NO_3^-}$ (R_9)	$Mn^{2+} + \frac{2}{5}NO_3^- + \frac{4}{5}H_2O \rightarrow MnO_2 + \frac{1}{2}N_2 + \frac{8}{5}H^+$
Iron oxidation by $\boldsymbol{NO_3^-}$ (R_{10})	$Fe^{2+} + \frac{1}{5}NO_3^- + \frac{12}{5}H_2O \rightarrow Fe(OH)_3 + \frac{1}{10}N_2 + \frac{9}{5}H^+$
Fe-sulfide oxidation (R_{11})	$Fe(OH)_3 + \frac{1}{2}H_2S + 2H^+ \rightarrow Fe^{2+} + \frac{1}{2}S_0 + 3H_2O$
Mn-Iron oxidation (R_{12})	$MnO_2 + 2Fe^{2+} + 4H_2O \rightarrow 2Fe(OH)_3 + Mn^{2+} + 2H^+$
Precipitation reactions	
FeS precipitation (R_{13})	$Fe^{2+} + H_2S \rightarrow FeS + 2H^+$
Pyrite pathway (R_{14})	$FeS + H_2S \rightarrow FeS_2 + H_2$
$MnCO_3$ precipitation (R_{15})	$Mn^{2+} + CO_2 + H_2O \rightarrow MnCO_3 + 2H^+$
$FeCO_3$ precipitation (R_{16})	$Fe^{2+} + CO_2 + H_2O \rightarrow FeCO_3 + 2H^+$

a: N/C ratio (16/106).

Table 3
Rate expressions considered in the transport-reaction model.

ID	Rate expression	Units
R_1	$R_{TOC}\frac{[O_2]}{K_{O2}+[O_2]}$	mM/a of CH_2O
R_2	$R_{TOC}\frac{K_{O2}}{K_{O2}+[O_2]}\frac{[NO_3^-]}{K_{NO3}+[NO_3^-]}$	mM/a of CH_2O
R_3	$R_{TOC}\frac{K_{O2}}{K_{O2}+[O_2]}\frac{K_{NO3}}{K_{NO3}+[NO_3^-]}\frac{[MnO_2]}{K_{MnO2}+[MnO_2]}$	mM/a of CH_2O
R_4	$R_{TOC}\frac{K_{O2}}{K_{O2}+[O_2]}\frac{K_{NO3}}{K_{NO3}+[NO_3^-]}\frac{K_{MnO2}}{K_{MnO2}+[MnO_2]}\frac{[Fe(OH)_3]}{K_{Fe(OH)3}+[Fe(OH)_3]}$	mM/a of CH_2O
R_5	$R_{TOC}\frac{K_{O2}}{K_{O2}+[O_2]}\frac{K_{NO3}}{K_{NO3}+[NO_3^-]}\frac{K_{MnO2}}{K_{MnO2}+[MnO_2]}\frac{K_{Fe(OH)3}}{K_{Fe(OH)3}+[Fe(OH)_3]}\frac{[SO_4^{2-}]}{K_{SO4}+[SO_4^{2-}]}$	mM/a of CH_2O
R_6	$k_6[NH_4^+]\,[O_2]$	mM/a of NH_4^+
R_7	$k_7[Mn^{2+}]\,[O_2]$	mM/a of Mn^{2+}
R_8	$k_8[Fe^{2+}]\,[O_2]$	mM/a of Fe^{2+}
R_9	$k_9[Mn^{2+}]\,[NO_3^-]$	mM/a of Mn^{2+}
R_{10}	$k_{10}[Fe^{2+}]\,[NO_3^-]$	mM/a of Fe^{2+}
R_{11}	$k_{11}\,[Fe(OH)_3][H_2S]$	mM/a of $Fe(OH)_3$
R_{12}	$k_{12}\,[MnO_2][Fe^{2+}]$	mM/a of MnO_2
R_{13}	$k_{13}[Fe^{2+}]\,[H_2S]$	mM/a of Fe^{2+}
R_{14}	$k_{14}[FeS]\,[H_2S]$	mM/a of FeS
R_{15}	$k_{15}[Mn^{2+}]\,[CO_3^{2-}]$	mM/a of Fe^{2+}
R_{16}	$k_{16}[Fe^{2+}]\,[CO_3^{2-}]$	mM/a of Mn^{2+}

Table 4
Reaction terms for species used in the transport-reaction model.

Species	Symbol	Unit	Reaction term $\sum \boldsymbol{R_i}$
Total organic carbon	$\boldsymbol{CH_2O}$	mmol/dm^{-3}	$-\boldsymbol{R_{TOC}}$
Oxygen	O_2	mM	$-f_cR_1-2R_6-\frac{1}{2}R_7-\frac{1}{4}R_8$
Nitrate	NO_3^-	mM	$-\frac{4}{5}f_cR_2+R_6-\frac{2}{5}R_9-\frac{1}{5}R_{10}$
Ammonium	NH_4^+	mM	$f_caR_{TOC}-R_6$
Dissolved manganese	Mn^{2+}	mM	$2f_cR_3-R_7-R_9+f_cR_{12}-R_{15}$
Dissolved iron	Fe^{2+}	mM	$2f_cR_4-R_8-R_{10}+f_cR_{11}-2f_cR_{12}-R_{13}-R_{16}$
Sulphate	SO_4^{2-}	mM	$-\frac{1}{2}f_cR_5$
Total hydrogen sulfide	ΣH_2S	mM	$\frac{1}{2}f_cR_5-\frac{1}{2}f_cR_{11}-R_{13}-f_cR_{14}$
Dissolved inorganic carbon	ΣCO_2	mM	$f_cR_{TOC}-R_{15}-R_{16}$
Manganese oxide	MnO_2	mM	$-2R_3+\frac{1}{f_c}R_7+\frac{1}{f_c}R_9-R_{12}$
Iron oxide	$Fe(OH)_3$	mmol/dm^{-3}	$-4R_4+\frac{1}{f_c}R_8+\frac{1}{f_c}R_{10}-R_{11}-2R_{12}$
Iron monosulfide	FeS	mmol/dm^{-3}	$\frac{1}{f_c}R_{13}-R_{14}$
Manganese carbonate	$MnCO_3$	mmol/dm^{-3}	$\frac{1}{f_c}R_{15}$
Siderite	$FeCO_3$	mmol/dm^{-3}	$\frac{1}{f_c}R_{16}$

of the bulk organic matter and its evolution within the sediment is related to the reactivity of each class by $\overline{k}=\sum_{i=1}^{3}\sigma_i C_{org}^i/\sum_{i=1}^{3}C_{org}^i$.

The boundary conditions at the SWI and at 25 cm sediment depth are imposed concentrations and fluxes for the aqueous and solid species (Table S1). Three different TOC fluxes (F_{org1}, F_{org2} and F_{org3}) are applied at the upper boundary (SWI). The benthic TOC flux at the SWI is then calculated as the sum of these fluxes.The stable carbon isotopic composition of DIC was calculated from the modelled ratio R = [DI^{13}C]/[DI^{12}C] relative to the ratio R_{VPDB} of the Vienna Peedee Belemnite standard (VPDB) according to:

$$\delta^{13}C=\frac{R-R_{VPDB}}{R_{VPDB}}\cdot 1000\ [‰] \quad (6)$$

The absolute concentrations of [DI^{13}C] and [DI^{12}C] were computed by separate reaction-transport equations for each isotope. Negligible carbon isotope fractionation was assumed during organic carbon degradation and carbonate precipitation (Meister et al., 2019). Therefore, the source of DIC was assumed to show the same isotopic composition as the organic carbon source pool, which was deduced from Miller-Tans plots (Müller et al., 2025).

The model was coded in R (version 3.2.4) using the ReacTran package (Soetaert and Meysman, 2012) to solve E and 2 and the marelac package (Soetaert et al., 2010) to solve the molecular diffusion coefficients for the modelled species (D_0). An unevenly spaced grid was used, with a grid size increasing downcore from the SWI to the maximum simulated depth of 25 cm, controlled by a power factor (p. dx.1 = 1.005 in "setup.grid.1D″ function within the ReacTran package). The finest grid size at the SWI is 10^{-6} cm and the coarsest grid size is 0.124 cm at 25 cm. The partial differential equations (PDEs; Eqs. (1) and (2)) were solved using "steady.1D″ with the solver "stode" within the ReacTran package.

The DOU used for re-oxidation of reduced metabolites from anaerobic remineralisation of OC is calculated by the depth integration of the oxidation rates R_6, R_7 and R_8 (Tables 2 and 3).

To account for the transient state conditions caused by the storm-induced pore-water mixing at four sites in the shallow eastern HMA – namely sites NE, E, SC and SE (Müller et al., 2025) – we used site SC as a type example and applied the model in a transient state. First, the model was run until a steady state was reached at site SC. Then pore-water concentrations in the upper 1, 2, 5, 10 and 15 cm, respectively, were replaced by those of bottom water to mimic the effect of the storm-induced pore-water mixing. All other parameters and boundaries were kept unchanged and the transient-state model was run for 30 days. This approach allowed us to quantify the relative differences in degradation rates and pathways compared to the steady state at different solute mixing depths (1, 2, 5, 10, 15 cm) and at different times (t = 5, 10, 20 and 30 days) after the mixing event. The results of these simulations were then used to correct the rates of the pathways of the steady-state model to account for the time between the storm-induced pore-water mixing and the sampling of the surface sediments. The PDEs in the transient model were solved by the function "ode.1D" with the solver "lsode" within ReacTran package. The differences between the measured and calculated concentrations/values C_{mea}^i and C_{calc}^i at each depth i were calculated using the mean square error (MSE) as:

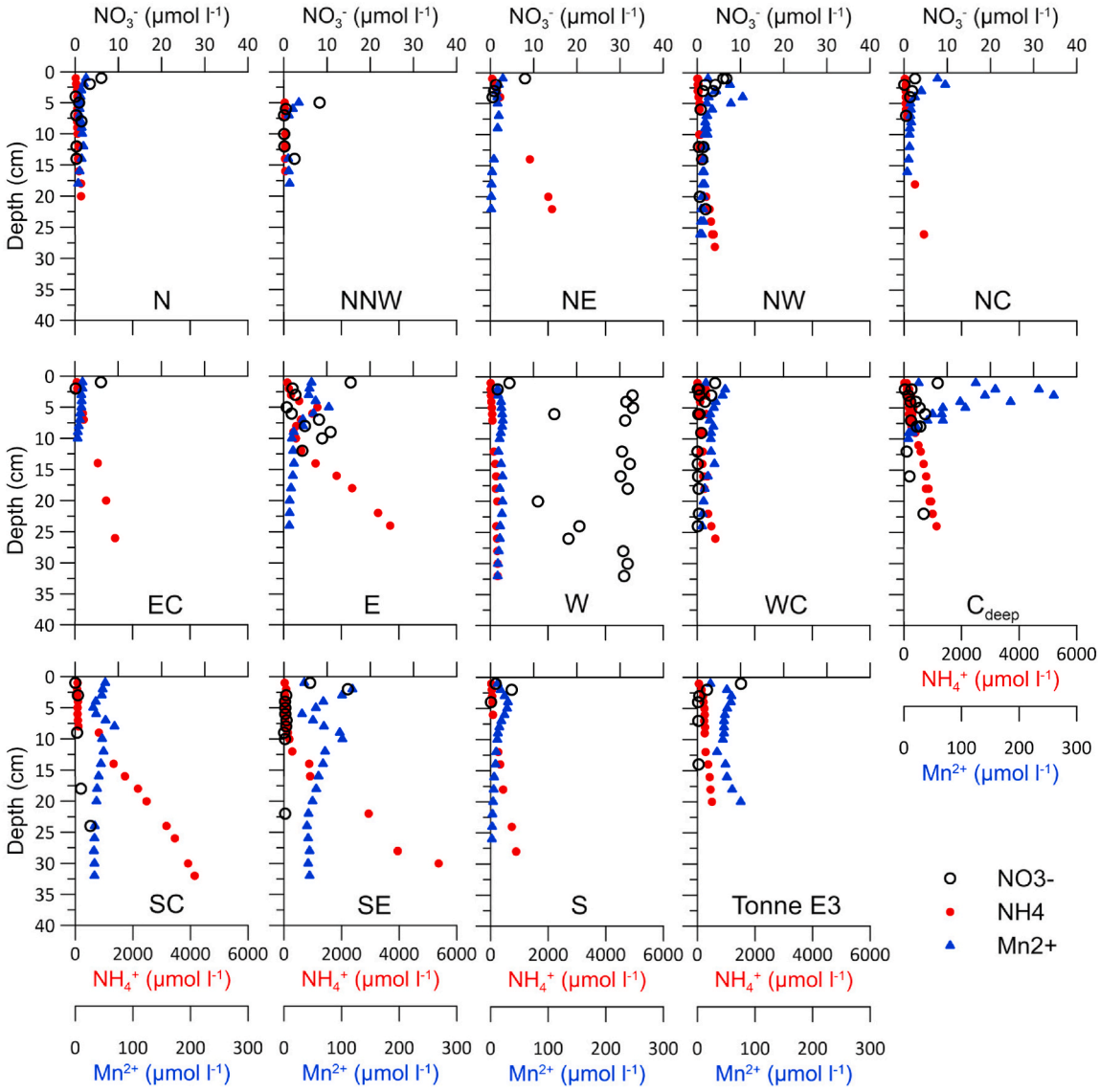

Fig. 2. Pore-water profiles of nitrate (NO_3^-), ammonia (NH_4^+) and dissolved manganese (Mn^{2+}) concentrations. For site names, see Table 1.

$$MSE = \frac{1}{N}\sum_{i=1}^{N}\left(\frac{C^i_{mea} - C^i_{calc}}{C^i_{mea}}\right)^2 \quad (7)$$

The minimised sum of the MSE for all porewater concentrations was used to find the best fitting parameters.

4. Results

4.1. Pore water: results of chemical analyses

At most sampling sites – except for sites NC and SC – characteristic subsurface nitrate peaks of up to 15 µmol l^{-1} are determined in the upper 5 cm of the sediments. A more scattered pattern of NO_3^- concentrations is observed at sites E and W, with site W showing overall highest nitrate concentrations of about 30 µmol l^{-1} throughout the core. Except for sites N, NNW and W, pore-water NH_4^+ concentrations generally increase with depth at all sites (Fig. 2). The steepest concentration gradients are found at sites NE, E, SC and SE, with the highest concentrations of up to 5400 µmol l^{-1} at site SE. Downward-increasing NH_4^+ concentrations are also observed at sites NW, NC, EC, WC, C_{deep}, S and Tonne E3. However, here, the concentrations are lower and do not exceed 1500 µmol l^{-1}. In contrast to the increasing NH_4^+ concentrations with depth at most sites, no clear trend in NH_4^+ concentrations is found at sites N, NNW and W (Fig. 2).

Dissolved Mn increases from the SWI downcore at most sites and peaks within the upper 5 cm of the sediments. Highest Mn^{2+} concentrations of 260 µmol l^{-1} are found at site C_{deep} (Fig. 2). At sites SC and SE, a second peak is observed between 7.5 and 10 cm, respectively. At site Tonne E3, dissolved Mn increases further downcore below 12 cm, below the upper Mn peak. Overall lowest Mn^{2+} concentrations throughout the core are found at sites N and NE. Pore-water Fe^{2+} profiles show a similar pattern to the Mn^{2+} profiles, with a peak in the upper 10 cm of the sediments and around similar depths as the Mn^{2+} peaks (Fig. 3). The overall highest Fe^{2+} concentrations are found at site C_{deep} amounting to 172 µmol l^{-1}. At sites E and SE, a second peak in Fe^{2+} is found at 22 and 27 cm, respectively. At sites E and Tonne E3 dissolved iron is present over the whole length of the cores.

Except for site NNW, all other 13 sites show a downward decrease in SO_4^{2-} concentrations from ~26 mmol l^{-1} at the SWI to varying concentrations at the bottom of the core ranging from ~24 mmol l^{-1} at site N, W and Tonne E3 to close to 0 mmol l^{-1} at sites SC and SE (Fig. 3). At sites N, NW, NC, EC, W, WC, C_{deep}, S and Tonne E3 sulphate concentrations decrease linearly with depth or show a slightly concave-down shape. In contrast, sites NE, E, SC and SE located in the eastern

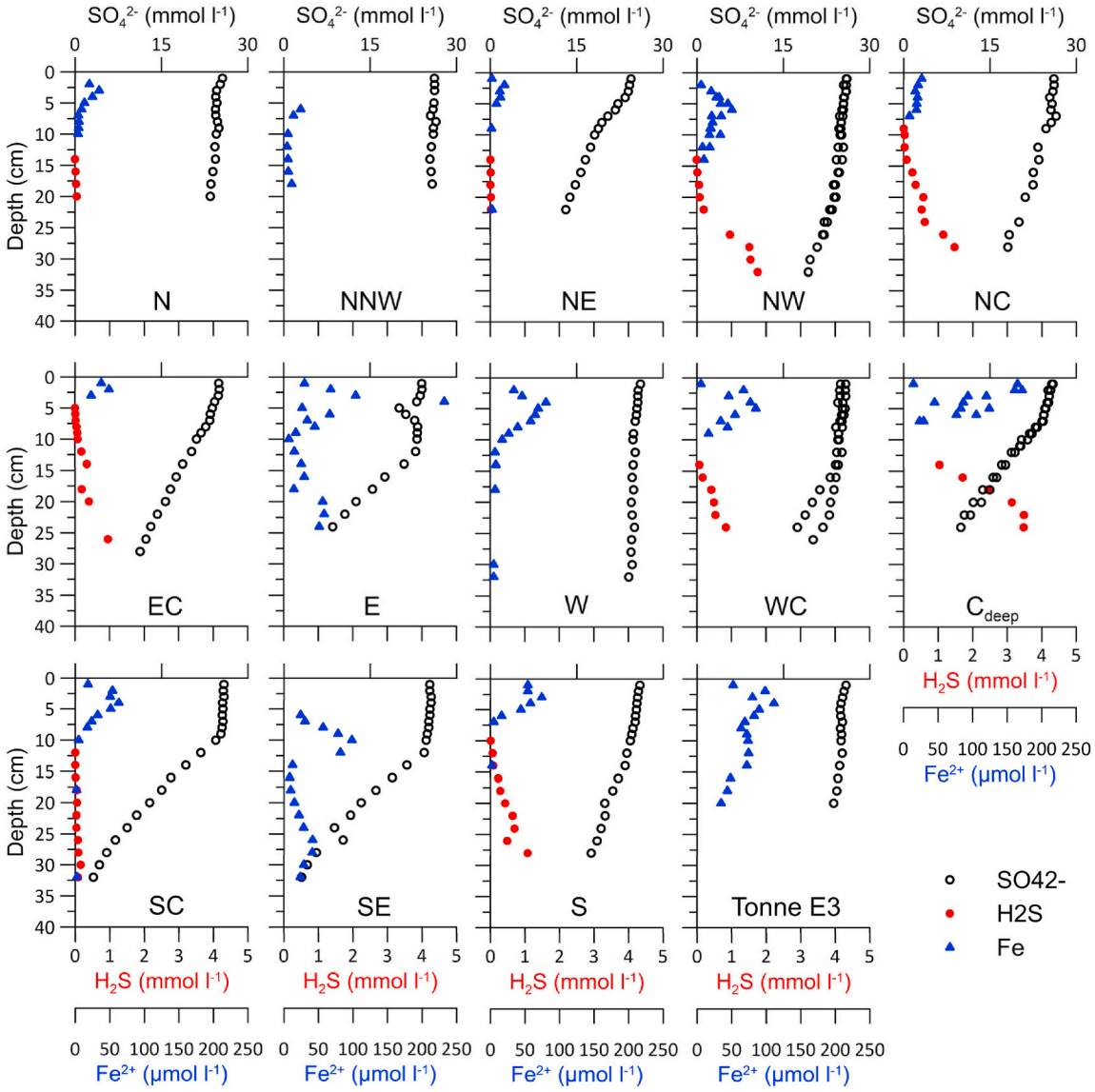

Fig. 3. Pore-water profiles of dissolved iron (Fe^{2+}), sulphate (SO_4^{2-}) and sulfide (H_2S) concentrations. For site names, see Table 1.

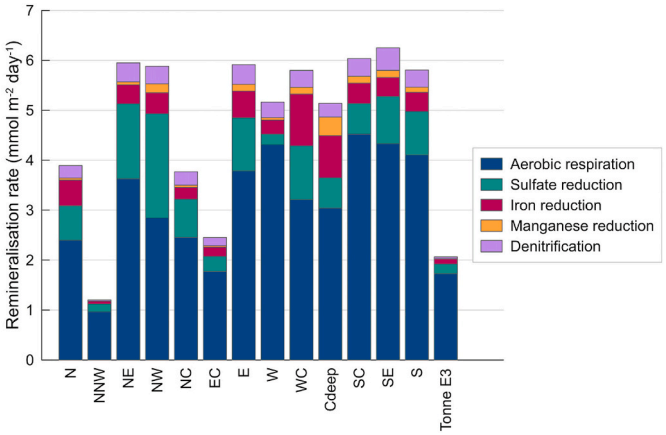

Fig. 4. Result of the steady state full diagenetic model. Different pathways of organic carbon remineralisation cumulating to the total remineralisation rate. For site names see Table 1.

shallow water-depth area of the HMA, display rather constant SO_4^{2-} concentrations in the uppermost ~10 cm of the sediments and a linear downward decrease below. At site NNW constant SO_4^{2-} concentrations are found over the entire core. H_2S was only detectable at sites N, NE, NW, NC, EC, WC, C_{deep}, SC and S. While at sites NW, NC, EC, WC, C_{deep} and S hydrogen sulfide concentrations increase with depth below ~10 cm up to 3.5 mmol l^{-1}, at sites N and NE concentrations remain low (Fig. 3).

4.2. *Diagenetic modelling*

4.2.1. *Steady-state modelling*

The steady-state full diagenetic model as described above was applied using the pore-water and solid-phase data of all 14 sites to determine total remineralisation rates, respective remineralisation pathways, as well as OC fluxes to and DIC fluxes out of the sediment. The modelling was performed using the data presented in this study as well as porosities, sedimentation rates, TOC contents, oxygen profiles, DIC and δ^{13}C-DIC data from Müller et al. (2025). As the data for the dumping site for harbour sludge Tonne E3, located in the south-western HMA, were not part of the study by Müller et al. (2025), the relevant data for the parameters mentioned above are included in this study.

Table 5
Rates of the different pathways of organic carbon remineralisation, organic carbon flux to the sediment-water interface, average organic carbon reactivity of the flux, total remineralisation rate and DIC flux across the sediment-water interface, derived from the full diagenetic model. Note that the corrected values considering the transient conditions at sites NE, E, SC and SE are shown, with the uncorrected values of the steady-state results given in brackets.

Site name	Aerobic respiration (mmol m^{-2} day^{-1})	SO_4^{2-} reduction (mmol m^{-2} day^{-1})	Fe^{2+} reduction (mmol m^{-2} day^{-1})	Mn^{2+} reduction (mmol m^{-2} day^{-1})	Denitrification (mmol m^{-2} day^{-1})	Benthic OC flux (mmol m^{-2} day^{-1})	Average reactivity (yr^{-1})	Total remineralisation (mmol m^{-2} day^{-1})	DIC flux (mmol m^{-2} day^{-1})
N	2.4	0.7	0.5	0.0	0.2	8.5	3.9	3.9	4.1
NNW	1.0	0.2	0.1	0.0	0.0	2.6	3.2	1.2	1.1
NE	3.6 (3.6)	1.7 (1.5)	0.4 (0.4)	0.1 (0.1)	0.3 (0.4)	7.7	7.1	5.9	8.1
NW	2.8	2.1	0.4	0.2	0.4	10.3	5.3	5.9	6.5
NC	2.5	0.8	0.2	0.0	0.3	7.7	3.6	3.8	4.7
EC	1.8	0.3	0.2	0.0	0.2	3.6	4.6	2.5	3.8
E	3.8 (3.8)	1.2 (1.1)	0.6 (0.5)	0.1 (0.1)	0.3 (0.4)	7.7	7.1	5.9	9.3
W	4.3	0.2	0.3	0.0	0.3	11.8	4.2	5.2	5.2
WC	3.2	1.1	1.0	0.1	0.3	10.7	5.1	5.8	6.3
C_{deep}	3.0	0.6	0.8	0.4	0.3	9.0	4.5	5.1	7.2
SC	4.5 (4.5)	0.7 (0.6)	0.5 (0.4)	0.1 (0.1)	0.3 (0.4)	17.8	3.1	6.0	10.4
SE	4.3 (4.3)	1.1 (0.9)	0.4 (0.4)	0.1 (0.1)	0.3 (0.5)	14.2	3.8	6.3	12.2
S	4.1	0.9	0.4	0.1	0.3	9.3	5.9	5.8	6.8
Tonne E3	1.7	0.2	0.1	0.0	0.0	3.6	4.6	2.1	2.0

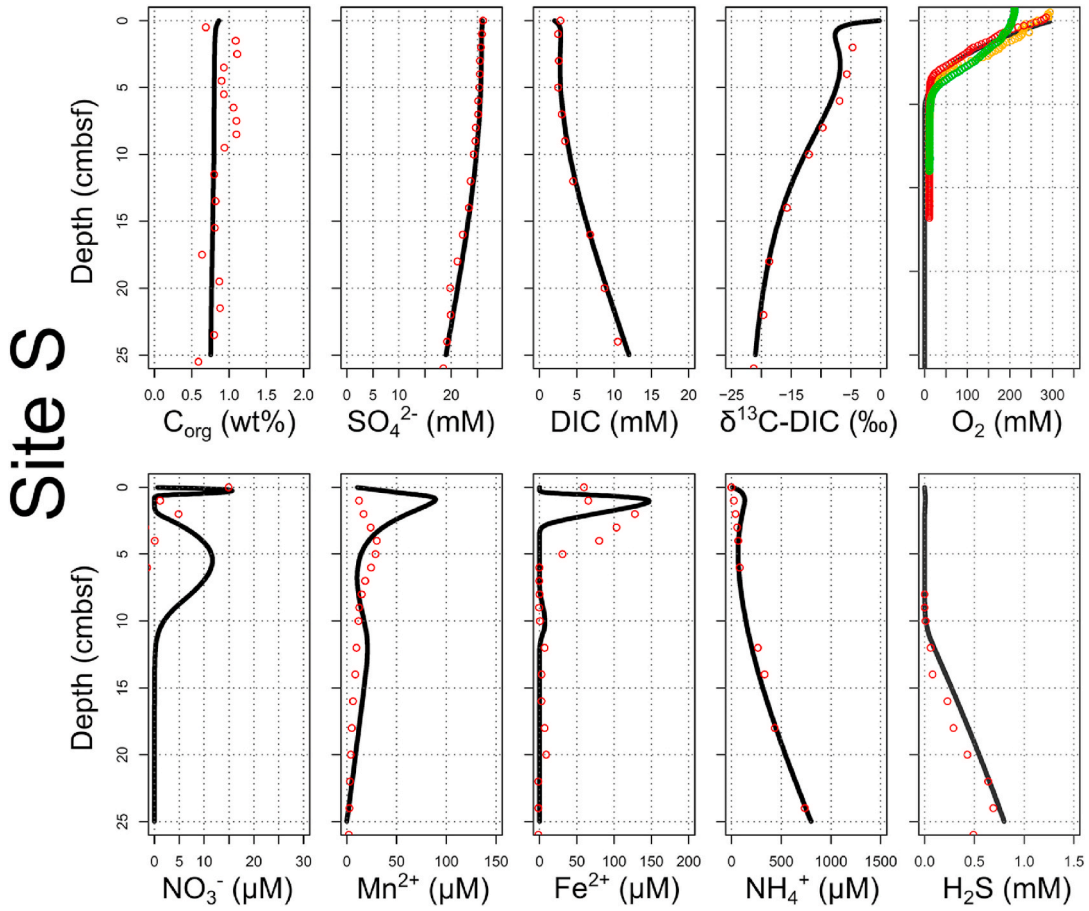

Fig. 5. Example of the best fit of the steady-state model for site S. Open circles are the measured values and the black lines are the model results. Multiple oxygen concentration measurements are displayed in different colours. Best fit parameterisations of the model for all sites are given in Table S1. (For interpretation of the references to colour in this figure legend, the reader is referred to the Web version of this article.)

The best-fit parameters are shown in Table S1 and the resulting rates are shown in Fig. 4 and Table 5. An example of the model results for site S is given in Fig. 5, the other results are shown in Fig. S2–S14. The best-fit **benthic OC fluxes** towards the SWI show a range from 2.6 to 17.8 mmol m^{-2} day^{-1}. Highest values are determined at sites SC and SE (Fig. 6a). The assumed weighted **average reactivity** of the OC-pool at the SWI (hereafter: average reactivity of the OC at the SWI) ranges from 3.1 yr^{-1} to 7.1 yr^{-1}. Highest reactivities of 7.1 yr^{-1} are found at sites NE and E in the shallow eastern HMA (Fig. 6c). Intermediate reactivities of 4.2–5.9 yr^{-1} are determined for sites NW, EC, W, WC, C_{deep}, S, Tonne E3 in the deeper western HMA and in the eastern central HMA. Overall lowest reactivities ranging between 3.1 and 3.9 yr^{-1} are found in the

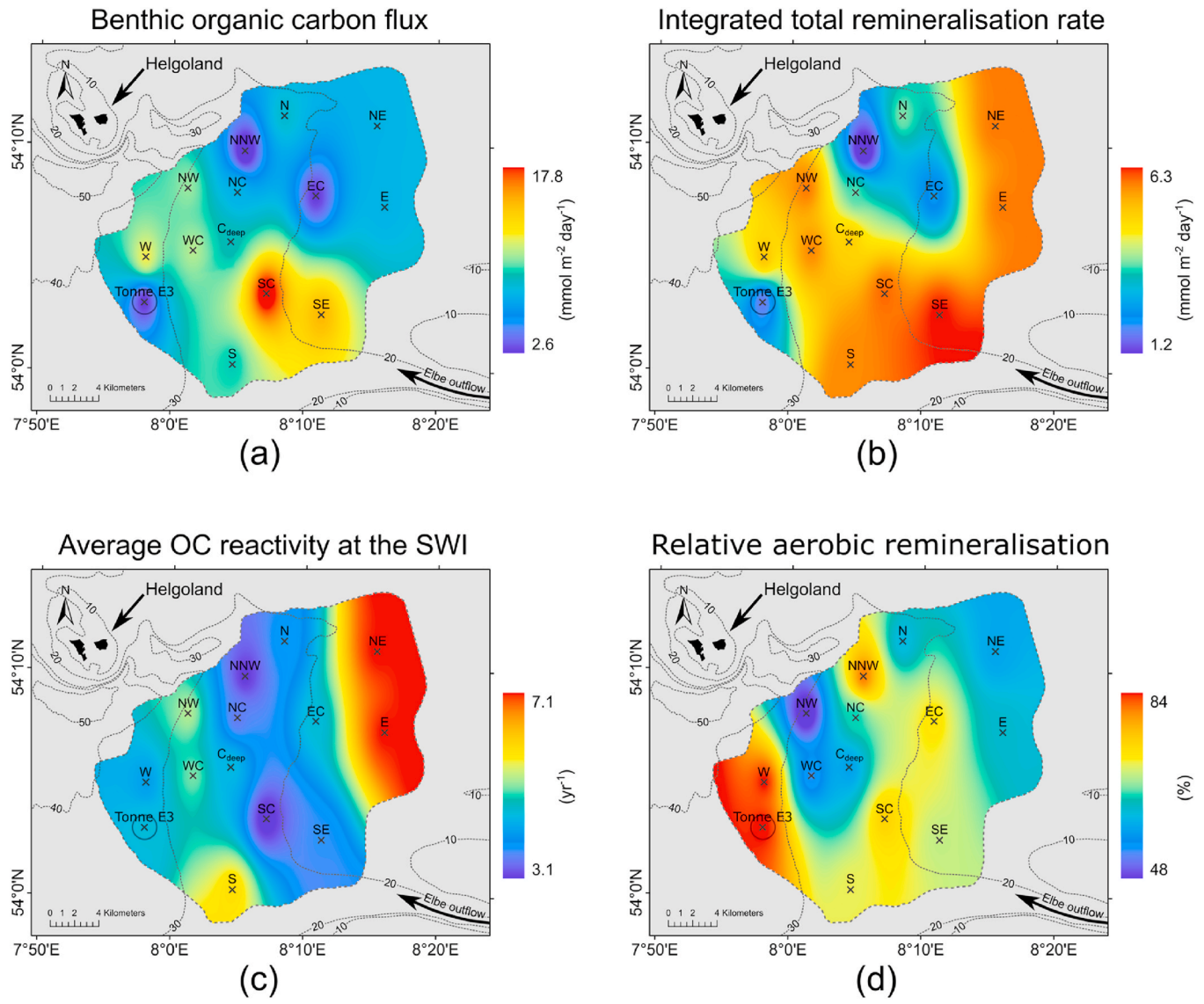

Fig. 6. Interpolated (a) benthic organic carbon fluxes, (b) integrated total remineralisation rates of the upper 25 cm of the sediments, (c) average reactivities of the benthic organic carbon fluxes and (d) relative contribution of aerobic remineralisation to total remineralisation. Interpolations were performed using the inverse distance weighted tool within ArcGIS Pro (version 3.3). For site names see Table 1.

southern, central and northern parts of the HMA, namely at sites N, NC, NNW, SC and SE.

Integrated **total OC remineralisation** rates vary by a factor of five across the HMA and range from 1.2 to 6.3 mmol m^{-2} day^{-1} (Fig. 6b). High values between 5.1 and 6.3 mmol m^{-2} day^{-1} are determined for most parts of the HMA (sites: NE, NW, E, W, WC, C_{deep}, SC, SE, S). Sites with lower values of 1.2–3.9 mmol m^{-2} day^{-1} are located in the northern and northern-central HMA (sites: N, NNW, NC, EC) as well as for site Tonne E3. The **OC burial efficiencies** obtained from the full diagenetic model vary between 22 and 66 % in the HMA. The highest OC burial efficiencies are found in the southern, central and northern parts of the HMA (sites: N, NNW, NC, SC, SE) and at site W in the deeper HMA, where values range from 51 to 66 %. Intermediate OC burial efficiencies of 38–46 % are found in the northwestern, west-central and southern HMA (sites: NW, WC, C_{deep}, S, Tonne E3). Overall lowest OC burial efficiencies of 22–31 % are determined for the shallow-water sites in the eastern HMA (sites: NE, EC, E).

The **DIC fluxes** across the SWI into the bottom water range from 1.1 to 12.2 mmol m^{-2} day^{-1}. Benthic DIC fluxes across the HMA show highest values of 8.1–12.6 mmol m^{-2} day^{-1} in the shallow eastern HMA at sites NE, E, SC and SE, intermediate fluxes of 5.2–7.2 mmol m^{-2} day^{-1} in the central and deeper western HMA, and lowest fluxes between 1.1 and 4.7 mmol m^{-2} day^{-1} in the northern and north-central HMA (sites N, NNW, NC, EC) as well as at site Tonne E3 in the southwestern HMA. Based on the steady-state model, **aerobic respiration** shows high values at all sites ranging from 1.0 to 4.5 mmol m^{-2} day^{-1} and contributes on average 66 % to the total OC remineralisation. The spatial distribution of aerobic respiration rates shows highest values of 3.6–4.5 mmol m^{-2} day^{-1} in the southern and shallow-water eastern HMA (sites: NE, E, W, SC, SE, S) as well as at site W in the deeper western HMA. Intermediate rates of 2.5–3.2 mmol m^{-2} day^{-1} are found in the central and north-western HMA (sites: NW, NC, WC and C_{deep}) and lowest rates of 1.0–2.4 mmol m^{-2} day^{-1} in the northern and north-central HMA (sites: N, NNW, EC) as well as at site Tonne E3.

Except for sites W and C_{deep} **sulphate reduction** at all other 12 sites is the second most important pathway contributing on average 17 % to the total OC remineralisation, ranging from 0.2 to 2.1 mmol m^{-2} day^{-1}. The sites with the highest sulphate reduction rates are sites NW and NE with 2.1 and 1.5 mmol m^{-2} day^{-1}, respectively. Sulphate reduction rates between 0.6 and 1.1 mmol m^{-2} day^{-1} are found for large parts of

the southern, eastern and central HMA, namely sites N, NC, E, WC, C_{deep}, SC, SE, S. The lowest sulphate reduction rates of 0.2–0.3 mmol m^{-2} day^{-1} are found in the northwestern, east-central and western HMA (sites: NNW, EC, W, Tonne E3). **Iron reduction** contributes on average 8.8 % to the total OC remineralisation and iron reduction rates range between 0.1 and 1.0 mmol m^{-2} day^{-1}. At sites WC and C_{deep} in the deeper central HMA, iron reduction is the second most important pathway of OC remineralisation and shows the overall highest values in the HMA of 1.0 and 0.8 mmol m^{-2} day^{-1}, respectively. In large parts of the HMA (sites: N, NE, NW, E, SC, SE, S) iron reduction ranges between 0.4 and 0.5 mmol m^{-2} day^{-1}, with lower values of 0.1–0.3 mmol m^{-2} day^{-1} only in the north-central and western HMA (sites: NNW, NC, EC, W, Tonne E3). **Denitrification** rates show values between 0.3 and 0.5 mmol m^{-2} day^{-1} in most of the HMA (sites: NE, NW, NC, E, W, WC, C_{deep}, SC, SE, S). Lower denitrification rates of 0–0.2 mmol m^{-2} day^{-1} were found only in the northern and eastern-central HMA (sites: N, NNW, EC) and at the site Tonne E3. Overall denitrification contributes on average 6.0 % to total OC remineralisation. **Manganese reduction** plays the least important role in OC remineralisation in the sediments of the HMA, contributing on average only 2.2 % to total remineralisation. Only the two sites NW and C_{deep} show manganese reduction rates higher than 0.1 mmol m^{-2} day^{-1} – namely 0.2 and 0.4 mmol m^{-2} day^{-1}, respectively. At all other 12 sites, manganese reduction rates are low and fluctuate between 0 and 0.1 mmol m^{-2} day^{-1}.

4.2.2. *Transient modelling*

Site SC was chosen as a representative site to assess the impact of transient state conditions at sites NE, E, SC and SE on the determination of the rates and metabolic pathways of OC remineralisation based on the full diagenetic model. Müller et al. (2025) demonstrated that non-steady-state conditions prevail at these sites – namely, pore-water mixing in the uppermost ~ 10 cm of the sediments caused by several intense storms that occurred three to four weeks before the expedition and sediment sampling took place (for discussion see section 5.1). To address this pore-water mixing, the transient state is evaluated for different pore-water mixing depths and different time steps after the tentative mixing event. The results show no changes in total remineralisation rates, but different relative changes in the different pathways of OC remineralisation for the distinct mixing depths and time steps after the mixing event (Fig. 7). At the greatest simulated mixing depth of 15 cm and at the first evaluated time step of five days after the mixing event the model shows the largest relative changes for each of the pathways. The relative rate changes compared to the steady state results for aerobic respiration, sulphate reduction, iron reduction, manganese reduction and denitrification are +14 %, −77 %, −85 %, −69 % and +77 %, respectively, for the greatest mixing depth of 15 cm after five days of simulation (Fig. 7). The smallest changes in rates for each pathway are between 0 and 1 % and are found for the lowest mixing depth of 1 cm after 30 days of simulation (Fig. 7). To correct for the storm-induced pore-water mixing (solute mixing depth of 10 cm) that occurred about 30 days before our sampling campaign with RV Heincke in March and April 2022 (for discussion see section 5.1), we use the determined relative changes of the transient model to correct the rates of each pathway derived from the steady-state model. We correct for the bias of

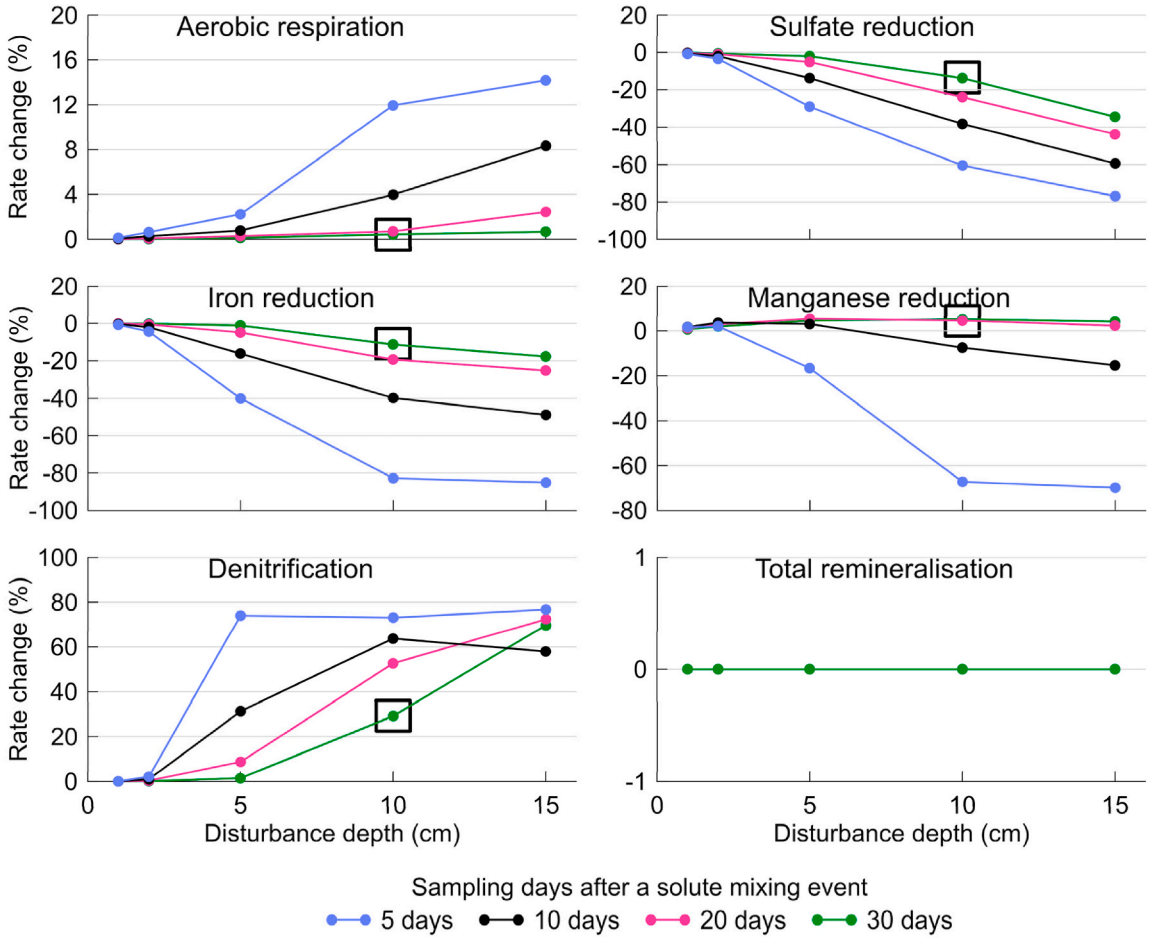

Fig. 7. Result of the case study on pore-water mixing. Relative rate changes compared to a steady state scenario at 5, 10, 20 and 30 days after a solute mixing event, where bottom water is mixed with pore water for different disturbance depths (solute mixed layer) at site SC. The scenario used to evaluate the impact of sampling time on the metabolic pathways is indicated as black boxes (30 days after a pore-water mixing event; 10 cm disturbance depth).

the steady-state modelled pathways caused by the change in pore-water profiles due to storm-induced pore-water mixing at sites NE, E, SC and SE for aerobic respiration, sulphate reduction, iron reduction, manganese reduction and denitrification by −0.4 %, 13.7 %, 11.3 %, −5.3 % and −29.2 % respectively. The overall contribution of the different pathways and their importance to total OC remineralisation remain about similar (Table 5).

5. Discussion

In the following, the influence of the different depositional conditions on the remineralisation rates of OC and its respective pathways in the sediments of the HMA will be discussed. We applied a full diagenetic model to quantify the benthic carbon fluxes, total OC remineralisation rates, the respective metabolic pathways and the fluxes of dissolved inorganic carbon across the sediment-water interface in the different depositional environments of the HMA. First, we assess which sites can be assumed to be in steady-state and which sites are in transient conditions. Müller et al. (2025) already provided indication that storm-induced mixing of pore water in the uppermost sediments caused by transient geochemical conditions at four sites in the shallow-water eastern HMA – namely at sites NE, E, SC and SE. The impact that these non-steady-state conditions have on determining rates and metabolic pathways of OC degradation will be quantitatively evaluated. Then we compare the results of the full diagenetic model with the previous calculations of total remineralisation rates, OC burial fluxes and benthic OC fluxes based on an empirical approach using DOU, sedimentation rates and TOC contents presented by Müller et al. (2025). We discuss the controls on the modelled total OC remineralisation rates derived from the full diagenetic model for the different environmental and depositional conditions presented by Müller et al. (2025). Then the influences of the different depositional factors and environments of the HMA on the respective pathways of OC remineralisation are evaluated. Additionally, we assess the impact of anthropogenic activities in areas of intense bottom trawling and dumping of harbour sediments on total remineralisation rates and metabolic pathways.

5.1. Sites at steady-state versus sites at non-steady-state

While pore-water data at most of the sites in the HMA indicate steady-state geochemical and depositional conditions, the four sites NE, E, SC and SE located in the eastern shallow-water area of the HMA display pore-water profile shapes (Fig. 3) that are indicative of transient conditions (e.g., Hensen et al., 2003; Kasten et al., 2003; Aller et al., 2010; Fischer et al., 2012; Henkel et al., 2012). This was already suggested by Müller et al. (2025) based on the pore-water profiles of DIC and δ^{13}C-DIC as well as radionuclide data. In short, DIC concentrations and δ^{13}C-DIC in the uppermost ~10 cm of the sediments show almost uniform concentrations close to those of bottom water. This is also supported by Miller-Tans plots, which show poor fits to the linear regression and values close to the bottom-water signature (Müller et al., 2025). In contrast, the $^{210}Pb_{xs}$ activity profiles decrease within the uppermost 10 cm and do not show a similarly mixed layer at these sites, indicating that only pore-water mixing has occurred without any significant mixing of the sediments (Müller et al., 2025). The sulphate data reported here (Fig. 3) further support this assumption by showing constant concentrations in the uppermost ~10 cm at sites NE, E, SC and SE.

In order to account for the impact that transient conditions of the storm-induced mixing of pore water with bottom water have on determining the rates and pathways of OC mineralisation, we selected site SC as a case study and applied a transient model. By applying this transient model, we were not only able to reproduce the measured pore-water profiles well, but also to quantify the effect of sampling time after the storm-induced pore-water mixing event on the remineralisation rates and the contribution of the different remineralisation pathways at these four sites. Although the storm-induced pore-water mixing is primarily indicated by DIC, δ^{13}C-DIC and sulphate profiles, it affects all remineralisation rates and pathways (Fig. 7; Video S1). The best fit between the pore-water concentration profiles of the transient model and the measurements at site SC is achieved with a mixing depth of pore water with bottom water of 10 cm, as expected by the pore-water concentration profiles, and a running time of the model of 30 days (Fig. 7, black boxes; Video S1). This corresponds well with the period between the series of winter storms in mid-February 2022 (Abromeit et al., 2022) and our sampling campaign with RV Heincke that was carried out in March and April 2022. The results of the transient model allow us to quantify the relative deviation of the rates of the different metabolic pathways compared to the rates derived from the steady-state model due to the storm-induced pore-water mixing. Based on the mixing scenario derived from site SC, we find that the oxygen profile readjusts rapidly after the storm-induced pore-water mixing event due to short diffusion distances as well as rapid re-oxidation of reduced substances and aerobic respiration. This results in only a slight overestimation of the aerobic respiration rate of 0.4 % in the steady state. The iron, manganese and sulphate profiles adjust intermediately due to lower reaction kinetics, resulting in a significant change of the sulphate, iron and manganese reduction rates, which are underestimated by 13.8 %, 11.3 % and overestimated by 5.2 %, respectively, in the steady state. The impact on the nitrate profile is the largest, and the denitrification rates recover the most slowly, due to the large amount of nitrate produced by nitrification. This leads to an overestimation of the denitrification rate of 29.2 % when considering steady state. The quantified relative effect of sampling time after the storm-induced pore-water mixing event on the pathways of OC remineralisation is applied to the four sites in the transient state – sites NE, E, SC and SE. In this way, we corrected for the effect of transient conditions on the determination of the rates and pathways of OC degradation.

In addition to the transient conditions in the shallow-water eastern HMA, site W is most likely also in a transient state, as indicated by the shape of the pore-water profiles that show fairly constant concentrations over depth in the uppermost 25 cm of the sediments (Figs. 2 and 3). Gravity core data collected during expeditions HE575 and HE595 in 2021 and 2022, respectively (Liu et al., in prep.), at the same site show a “downward-kink” shape of the sulphate concentration profile and a sulphate/methane transition zone that is located more than three times deeper in the sediments compared to the other sites. Both findings indicate non-steady state conditions to prevail at site W (e.g., Kasten et al., 2003; Haeckel et al., 2007; Aller et al., 2010; Santos et al., 2012) and hence the steady-state model results do not represent the transient conditions at site W. Additionally, in contrast to the transient conditions in the shallow water eastern HMA, the timing, depth and mechanism causing the transient conditions at site W are unknown. As a consequence, we cannot evaluate the respective pathways of OC mineralisation with our model setup (neither transient nor steady-state model) with high confidence and therefore exclude site W from the discussion on the remineralisation pathways below.

5.2. Remineralisation rates, OC burial and benthic OC fluxes – comparing the results of the full diagenetic model with the empirical approach

We first compare how well the empirical approach followed by Müller et al. (2025) agrees with the total remineralisation rates determined based on the full diagenetic model applied in this study. Müller et al. (2025) used DOU based on measured oxygen concentration profiles to estimate total remineralisation rates, assuming to reflect both aerobic remineralisation rates and re-oxidation of reduced solutes produced by anaerobic remineralisation processes (e.g., Glud, 2008). OC burial fluxes were estimated based on sedimentation rates and average TOC contents of the sediments and benthic OC fluxes as the combination of remineralisation and burial of OC. The only common parameter between both approaches is the sedimentation rate. The total remineralisation rates estimated by Müller et al. (2025) range from 1.3 to 25.8 gC

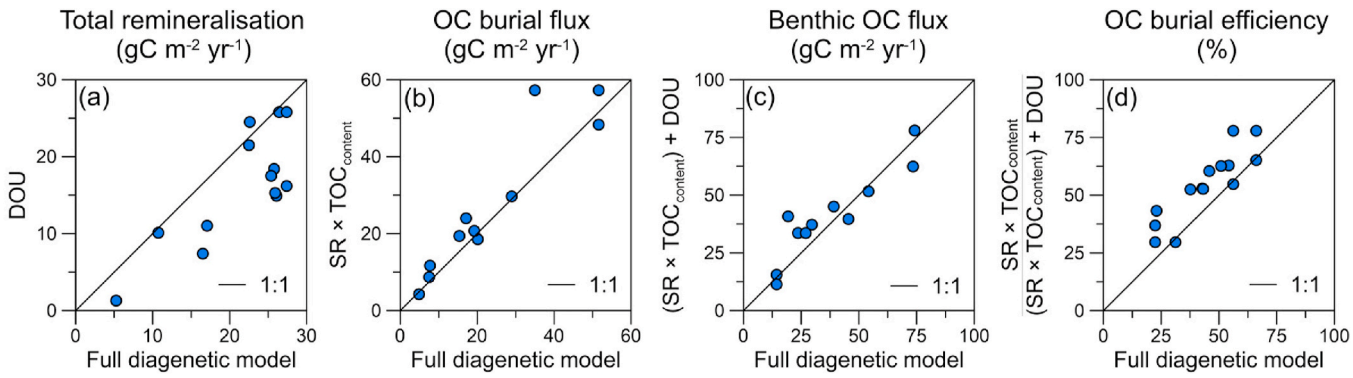

Fig. 8. Comparison between the steady state full diagenetic model (this study, x-axis) and the empirical approach (y-axis) presented by Müller et al. (2025). The black line is the 1:1 relation. (a) Total remineralisation rate estimated from dissolved oxygen uptake (DOU) vs. the full diagenetic model, (b) OC burial flux derived from sedimentation rate (SR) and total organic carbon content ($TOC_{content}$) vs. the full diagenetic model, (c) benthic carbon flux and (d) OC burial efficiency.

m^{-2} yr^{-1}, the rates determined based on the full diagenetic model range from 5.3 to 27.4 gC m^{-2} yr^{-1}. The results obtained from these two approaches generally agree well, but the rates derived from the full diagenetic model values are generally slightly higher than those calculated based only on the oxygen profiles (Fig. 8a). This might be caused by a slight imbalance in the re-oxidation of reduced metabolites released by anaerobic remineralisation pathways (e.g., Glud, 2008; Pastor et al., 2011). Using solely DOU does not consider processes like precipitation on these reduced metabolic products, whereas the full diagenetic model is capable of quantifying both aerobic and anaerobic processes (e.g., the production or re-oxidation of N_2 by denitrification, or the formation of FeS as an Fe^{2+} sink). OC burial fluxes and benthic OC fluxes calculated from the measured sedimentation rates, TOC contents and DOU show a very good agreement with the values derived from the full diagenetic model (Fig. 8b and c). The resulting OC burial efficiencies (the ratio of OC burial flux to benthic OC flux) are within a similar range of 29.7–77.9 % from the empirical approach and 22.4–61.1 % from the full diagenetic model. However, on average, OC burial efficiencies derived from the full diagenetic model are ~10 % lower than the empirically determined values (Fig. 8d), due to the slightly higher estimated total

Table 6
Benthic OC flux, average reactivity, total remineralisation rate, ratio of aerobic to total remineralisation and aerobic remineralisation contribution to total oxygen uptake (TOU) in other shelf environments.

Study area	Benthic OC flux (mmol m^{-2} day^{-1})	Average reactivity (yr^{-1})	Total remineralisation rate (mmol m^{-2} day^{-1})	Aerobic remineralisation/ total remineralisation (%)	Aerobic remineralisation/TOU (%)	Reference
Danish fjords, Kattegat, Skagerrak					50	Jørgensen (1982)
Gulf of Maine shelf	10.7					Christensen (1989)
Shelf off Chile		2.4–4.5				Thamdrup and Canfield (1996)
Off Nova Scotia			1–10			Grant et al. (1998)
Washington shelf			2.3–6.1			Kristensen et al. (1999)
Baltic Sea-North Sea transition	12.0–52.3		1.5–26.2			Jørgensen et al. (1990)
Ago Bay	14.7				47	Anggara Kasih et al. (2009)
Chesapeake Bay			2.2–19.7			Burdige et al. (2000)
Iberian shelf	2.2–9.4			60–90		Epping et al. (2002)
Northeast of Greenland					40	Berg et al. (2003)
Skagerrak, North Sea	11.8–41.7		2.2–18.0			Ståhl et al. (2004)
Mediterranean Sea shelf	9.6–65.5	5.7–31.0	4.6–25.1	8–67	63–93	Pastor et al. (2011)
Globally, <200 m water depth	0.6–35.9	0.03–24				Arndt et al. (2013)
Central North Sea shelf			4.0–13.5	59–90		De Borger et al. (2021)
European shelf, Arabian Sea	1.6–43.6	<0.01–0.25[a]				Freitas et al. (2021)
South Yellow Sea			5.1–18.8	53–67		Ren et al. (2022)
Shelf of the Antarctic Peninsula	2.5–13.0		0.1–7.4	63–94	16–74	Baloza et al. (2022)
Global assessment, shelf area		<0.01 - ~250[a]				Xu et al. (2023)
German Bight, SE North Sea	2.6–17.8	3.1–7.1	1.2–6.3	48–85	70–85	This study

[a] Reactivity at the sediment water interface.

remineralisation rates in the full diagenetic model (Fig. 8a).

As discussed and demonstrated above, both approaches provide similar results for total remineralisation rates, OC burial fluxes and benthic OC fluxes. While the empirical approach followed by Müller et al. (2025) provides a robust method for estimating total remineralisation rates as well as burial and benthic OC fluxes that requires only a few selected pore-water parameters and low computational effort, the full diagenetic model offers the possibility to quantify the contribution of the different metabolic pathways to the total OC degradation. In this way the full diagenetic model approach can thus also be applied/used to investigate the influence of the different depositional environments in the HMA on these pathways.

5.3. Controls on total OC remineralisation rates

Based on the full diagenetic model, we determined about a sevenfold variability in benthic OC fluxes to the SWI in the different sedimentary environments of the HMA (Table 5). These values are close to or indistinguishable from the ones reported by previous studies for the North Sea shelf and other shelf environments (Table 6). The highest benthic OC fluxes are found at sites SE and SC located in the southeast of the HMA (Fig. 6a). This area of the HMA is characterised by the highest sedimentation rates and a high deposition rate of terrestrial OC (Wei et al., 2025; Müller et al., 2025). In the western part of the HMA, where intermediate sedimentation rates and the burial of a larger fraction of OC of marine origin were shown to be present (Wei et al., 2025; Müller et al., 2025), benthic OC fluxes are higher than in the shallow eastern part of the HMA (Fig. 6a). The average reactivities of OC at the SWI are derived from the tuning parameters of the three OC fluxes (F_{TOC1}, F_{TOC2}, F_{TOC3}) and their respective reactivities (σ_1, σ_2, σ_3). The average reactivities of the benthic OC reaching the SWI in the HMA indicate a mixture between the reactivities of fresh marine OC and less reactive (resuspended, terrestrial) OC (e.g., Berner, 1980) and are comparable with, e.g., experimental work by Thamdrup and Canfield (1996) on the shelf off Chile, modelling work from the Mediterranean Sea shelf off France by Pastor et al. (2011) and the global assessment for water depth <200 m by Arndt et al. (2013) (Table 6).

The benthic OC flux in the HMA shows a positive correlation with sedimentation rates (Fig. 9a, Pearson correlation (cor) = 0.60, p = 0.02), while the average reactivity of the bulk OC supplied to the sediments is negatively correlated with sedimentation rate (Fig. 9b). The general trend of decreasing reactivity with increasing sedimentation rate reflects the dilution of labile OC (with high average reactivity) at higher sedimentation rates within the sediment matrix, analogue to findings by, e.g., Jung et al. (1997). The total remineralisation rates at lower benthic OC fluxes are lowest and increase up to a "threshold" maximum remineralisation rate of ~6 mmol m^{-2} day^{-1} at a benthic OC flux of around 10 mmol m^{-2} day^{-1} (Fig. 10a, Table 5). Total remineralisation rates do not further increase with increasing benthic carbon supply, as total remineralisation is not controlled by the amount of OC reaching the SWI but the availability of degradable OC (Fig. 9c). This results in similar total remineralisation rates of ~6 mmol m^{-2} day^{-1}, in large parts of the HMA, irrespective of the benthic carbon flux (Fig. 6b). We plotted the total remineralisation rates vs. benthic OC fluxes and fitted a logarithmic regression, for better visualisation (Fig. 10a). These total remineralisation rates are within the typical range reported for other shelf environments (Table 6). The DIC fluxes across the SWI into the bottom water are, on average, about 30 % higher than the determined total remineralisation rates, producing DIC by OC remineralisation (Table 5). Therefore, it is apparent that there is a second source of DIC besides OC remineralisation in the upper 25 cm of the sediments. The discrepancy between DIC fluxes and total remineralisation rates is caused by the integration of the total remineralisation rates in the upper 25 cm of the sediments, whereas DIC from below 25 cm sediment depth diffuses upwards and contributes to the total DIC flux at the SWI. Below 25 cm DIC could be formed during ongoing sulphate reduction, anaerobic oxidation of methane and methanogenesis.

The distribution of our modelled average reactivity of the benthic OC reaching the SWI shows an interesting pattern with lowest values in an area stretching from the southern HMA close to the river Elbe outflow towards the north along the slope of the HMA (Fig. 6c). Hertweck (1983) showed the degradation of less reactive – compared to marine OC – terrestrial OC using Miller-Tans plots. In this area, a turbidity maximum was observed in the water column, and it is speculated that constant tidal re-suspension of surface sediments increases the oxygen exposure time of the particulate organic carbon and results in the settling of high proportions of refractory POC (Hanz et al., in prep.). A detailed analysis of the effects of re-suspended matter is beyond the scope of this study and will be addressed in another study by Hanz et al. (in prep.). The largest differences in total remineralisation rates (Fig. 6b) and benthic OC fluxes (Fig. 6a), and thus the highest preservation of OC, occur at sites SC and SE in the southern HMA, and further north along the slope (Fig. 6, Table 5). These sites are characterised by the highest OC supply and low OC reactivity, resulting in OC burial fluxes of up to 11.8 and 8.0 mmol m^{-2} day^{-1} and burial efficiencies of up to 66 % and 56 % at sites SC and SE. In contrast, sites NE and E in the shallow eastern HMA have the highest average reactivities and relatively high remineralisation rates, leading to the lowest burial efficiencies of 22 % and 23 %, respectively. Thus, total OC remineralisation and burial in the HMA depend not only on benthic OC fluxes but also on the reactivity of the OC delivered to the seafloor.

5.4. The effect of different depositional environments on the remineralisation pathways

Aerobic respiration is the most important pathway of OC remineralisation in the sediments of the HMA ranging from 1.0 to 4.5 mmol m^{-2} day^{-1} and accounting for 48–85 % of total remineralisation (Table 5, Fig. 6d). These values are in a similar range as those determined on the North Sea shelf and other shelf environments with oxygen saturated

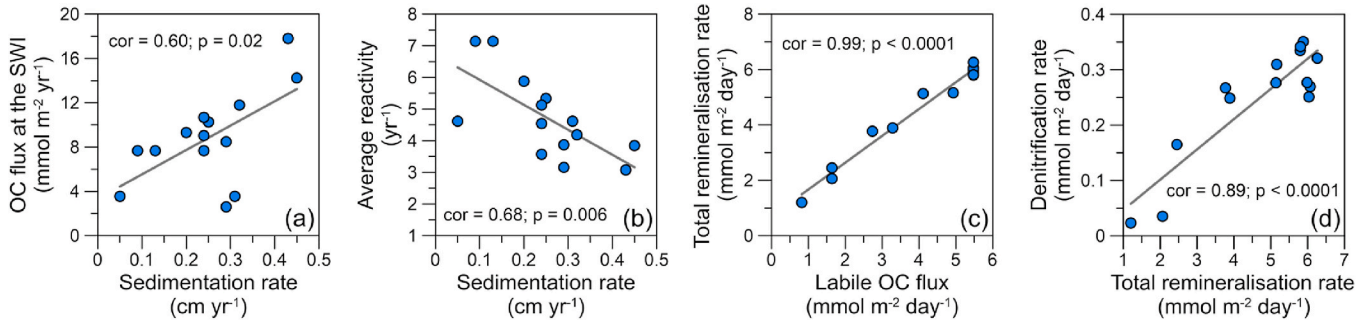

Fig. 9. Cross plots of (a) benthic OC reaching the sediment water interface vs. sedimentation rate, (b) average reactivity vs. sedimentations rate, (c) total remineralisation rate vs. the benthic flux of labile OC and (d) denitrification rate vs. the total remineralisation rate.

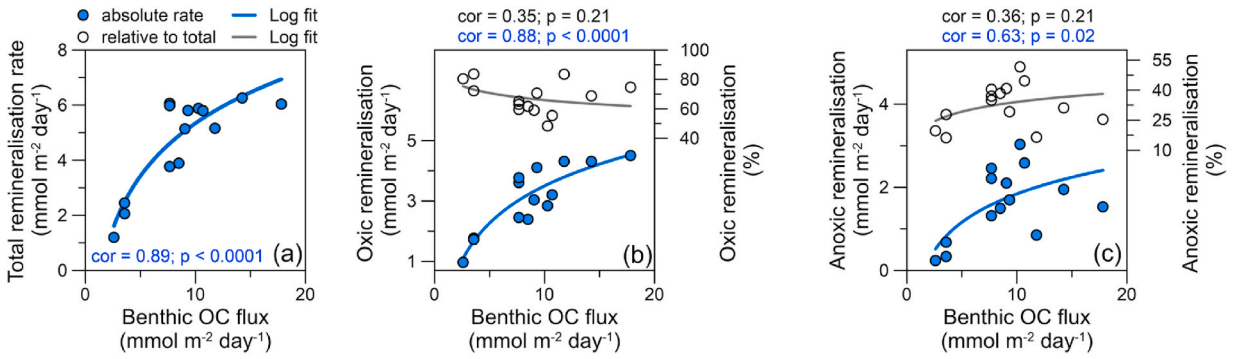

Fig. 10. Cross plots of (a) total remineralisation rates vs. benthic OC fluxes, (b) relative to total remineralisation (open circles) and absolute (blue dots) oxic remineralisation vs. benthic organic carbon fluxes and (c) relative to total remineralisation (open circles) and absolute (blue dots) anoxic remineralisation vs benthic organic carbon fluxes. (For interpretation of the references to colour in this figure legend, the reader is referred to the Web version of this article.)

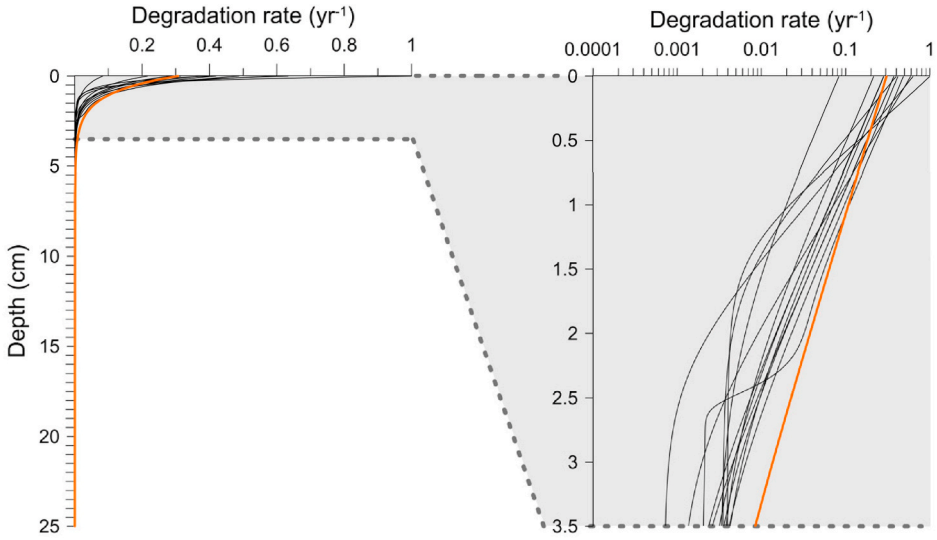

Fig. 11. Steady-state full diagenetic model result of the OC degradation rate (OC-pool weighted average OC reactivity) in the sediments. Note the different scales for the degradation rate: linear (left) and logarithmic (right). The orange line is the OC-pool weighted average reactivity distribution for site NW. The difference in OC-pool weighted average reactivity near the SWI is a result of the sediment mixing, which redistributes reactivities within the sediment even at very low mixing rates (cf. Fig. S1). (For interpretation of the references to colour in this figure legend, the reader is referred to the Web version of this article.)

bottom water (Table 6). Similar contributions of aerobic remineralisation have been reported for the central North Sea shelf by De Borger et al. (2021a), where only minor sediment accumulation occurs and profiles of nutrients e.g., ammonia, in the pore water indicate OC remineralisation being limited to the upper 4–6 cm of the sediments. In the sediments of the HMA, we find ammonia profiles that are slightly bent linear profiles (Fig. 2), indicating ongoing OC remineralisation in the sediments throughout the cores and below 25 cm sediment depth, similar to the indication in the DIC profiles. The high proportion of aerobic respiration to total OC remineralisation in the HMA, despite ongoing anaerobic remineralisation, can be explained by the vertical distribution of average OC reactivity in the sediments. We find that most of the labile OC is already degraded in the upper part of the sediment, hence the average reactivity decreases downward by an order of magnitude in the uppermost cm (Fig. 11). The preferential consumption of labile OC in the uppermost part of the sediments leaves less reactive OC available for anaerobic processes below as has been described previously (e.g., Jørgensen, 1982; Arndt et al., 2013; Mogollón et al., 2016; Middelburg, 2018 and references therein; Freitas et al., 2021; Xu et al., 2023). This results in a dominance of aerobic remineralisation rate compared to anaerobic remineralisation rates in the sediments of the HMA, despite a rather thin oxic layer. From the dissolved oxygen uptake (DOU) of the sediments in the HMA, aerobic respiration utilises about 79 % (70–85 %), whereas 15–30 % of DOU is used for re-oxidation of reduced metabolic products. The fraction of DOU for aerobic respiration in the HMA is higher than the 40 and 50 % reported for sediments of Danish fjords, the Kattegat, the Skagerrak, northeast off Greenland and the Ago Bay in Japan (Anggara Kasih et al., 2009; Berg et al., 2003; Jørgensen, 1982, Table 6). However, a similar value of 63–93 % is reported by Pastor et al. (2011) for sediments on the Mediterranean Sea shelf. Pastor et al. (2011) argue that the formation of e.g., FeS and FeS_2 represents a sink for reduced metabolic products in the sediments of their study area and thus results in a lower fraction of DOU used for re-oxidation. In our model, the authigenic iron sulfide mineral phases FeS and FeS_2 have been implemented as sinks for Fe^{2+} and HS^- as also demonstrated in numerous previous studies (e.g., Hensen et al., 2003; Riedinger et al., 2017). The DOU used for re-oxidation of reduced metabolites from anaerobic remineralisation of OC is dominated by the oxidation of ammonia, using on average 24.7 % of DOU, with smaller contributions from Fe^{2+} oxidation of 3.1 % and Mn^{2+} oxidation of 0.2 %. The vertical distribution of OC reactivity (cf. Fig. 11) in the sediments of the HMA also contributes to the low fraction of DOU used for re-oxidation, by limiting remineralisation and consequently the release of reduced metabolic products at depth.

The absolute and relative importance of aerobic and anaerobic remineralisation are generally controlled by water depth, subsequent

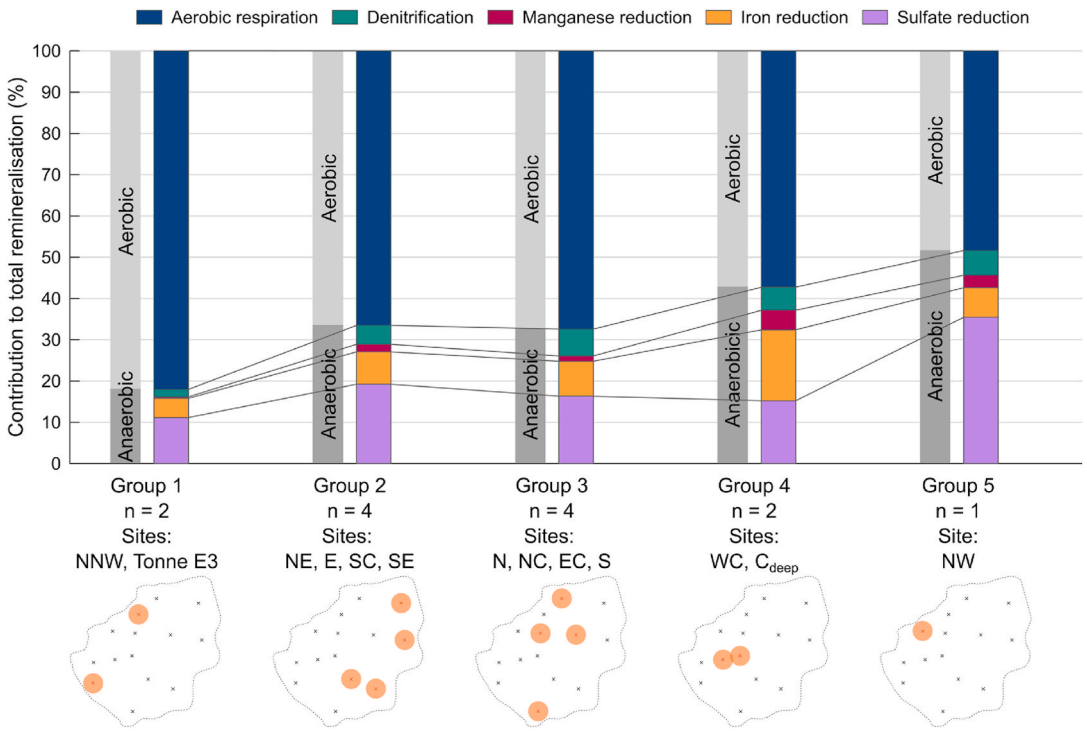

Fig. 12. Relative contribution of the different pathways to total remineralisation for all sites arranged in groups with similar contribution ranges. From left to right, the relative contribution of anoxic processes increases. At the bottom of the figure, the locations for each group in the HMA are highlighted.

benthic OC flux or directly to benthic OC flux and its reactivity (e.g., Jørgensen, 1982; Christensen, 1989; Thamdrup and Canfield, 1996; Pastor et al., 2011; Lipka et al., 2018; Baloza et al., 2022). As shown above, our data support the findings of increasing benthic OC flux enhancing total remineralisation rates (e.g., Christensen, 1989; Lipka et al., 2018). We find a strong significant correlation between benthic OC fluxes and absolute aerobic remineralisation rates (Fig. 10b) and a significant moderate correlation between benthic OC fluxes and absolute anaerobic remineralisation rates, but a more scattered pattern (Fig. 10c). However, there is no significant relationship between the relative contribution of aerobic and anaerobic processes to total OC remineralisation and the benthic OC flux (Fig. 10b and c), although benthic OC fluxes vary by almost an order of magnitude (Fig. 10b and c). Apart from sites NW and Tonne E3 that are impacted by anthropogenic activities (see discussion below) we find the highest contribution of aerobic respiration to total OC remineralisation at site NNW, where only little or no sedimentation is reported (von Haugwitz et al., 1988) and the mean grain size of 269 μm is comparatively high (Figge, 1981; Laurer et al., 2013; Bockelmann et al., 2018; Sievers et al., 2021; Wei et al., 2025). The coarse-grained sediments and the low flux of degradable OC to the SWI at site NNW result in a deep oxygen penetration depth of 3 cm (Müller et al., 2025). OC is exposed to oxygen for a long time due to little or no sediment accumulation (von Haugwitz et al., 1988), limiting anaerobic remineralisation in the upper 25 cm of the sediments to <20 % (Fig. 6d; Fig. 12, Group 1). The relative importance of aerobic respiration to total OC remineralisation of 69 % shows only a small variation of ±4 % in wide parts of the study area (Fig. 6d; Fig. 12, Groups 2, 3), with a lower aerobic contribution of ~57 % at sites WC and C_{deep} (Fig. 12, Group 4). Overall, the exposure time of OC to oxygen in the HMA appears to be long enough to degrade most of the reactive OC at all sites within the oxic layer, even at high benthic OC fluxes. This results in a rather uniform contribution of aerobic respiration to total remineralisation in the HMA.

Besides comparing aerobic and anaerobic processes, we can assess the influence of the different depositional conditions in the HMA on the different anaerobic metabolic pathways of OC remineralisation in more detail. In Fig. 12, sites with similar relative contribution of each metabolic pathway to total remineralisation are grouped to simplify the observations. The most important anaerobic pathway of OC remineralisation in the HMA is sulphate reduction (Fig. 12, Group 1, 2, 3, 5). Previous studies showed that the sulphate reduction rate is related to the sediment mass accumulation rate or the benthic OC flux (e.g., Henrichs and Reeburgh, 1987; Canfield, 1989; Pastor et al., 2011; Jørgensen, 2021; Baloza et al., 2022). In groups 2 and 3 (Fig. 12), with total remineralisation rates ranging from 2.5 to 6.3 mmol m^{-2} day^{-1}, we find increasing absolute sulphate reduction rates with increasing benthic OC flux, as also described by e.g., Jørgensen (2021) and references therein. Surprisingly, we do not find a relation between the relative contribution of sulphate reduction to total remineralisation in large parts of the HMA (Fig. 12, Group 2, 3). Groups 2 and 3 (Fig. 12) show similar relative contributions of sulphate reduction to total remineralisation of 16 ± 3 %, which is similar to the value approximated for shelf regions globally by Bowles et al. (2014). This value is about constant in the HMA (Groups 2 and 3), although covering a large range in several depositional parameters. Mud contents vary between 53 % and 93 % (Müller et al., 2025), sedimentation rates span almost one order of magnitude, 0.5–4.5 mm yr^{-1} (Müller et al., 2025), benthic OC fluxes show a factor of five difference from 3.6 to 17.8 mmol m^{-2} day^{-1}, average reactivities of the OC reaching the SWI vary between 3.1 and 7.1 yr^{-1} and total remineralisation rates vary between 2.5 and 6.3 mmol m^{-2} day^{-1}. This indicates that sulphate reduction in the HMA is not coupled to the magnitude of these parameters. Although the absolute sulphate reduction rates in group 4 are in a similar range of those in groups 2 and 3 (~0.8 mmol m^{-2} day^{-1}), the relative contribution of sulphate reduction in group 4 is lower. This is a result of the more than doubled rates of iron and manganese reduction in group 4, which also increases the contribution of total anaerobic remineralisation in group 4. In the largest groups 2 and 3, iron and manganese reduction contribute 8 ± 1 % and 2 ± <1 %, respectively, again almost equally for all sites and again spanning large parts of the HMA with a wide range of depositional conditions. The highest iron and manganese reduction rates in the HMA (group 4) are found near the site where high amounts of reactive iron

minerals in the sediments have been reported (e.g., lepidocrocite; Oni et al., 2015; Henkel et al., 2016, 2025). However, it is important to note that there is no comprehensive understanding of the distribution of reactive iron phases in the HMA. This only allows for speculation about the reasons or mechanisms controlling these higher rates. High iron and manganese reduction rates could either be the result of high fluxes of reactive iron and manganese into the sediments, or the result of higher sediment mixing rates. Higher amounts and fluxes of iron- and manganese-rich particles could originate from the estuaries of the rivers Weser and Elbe where the mixing of river water and seawater typically induces flocculation and the formation of high loads of suspended particles (e.g., Boyle et al., 1977), whereas higher sediment mixing rates enhance the cycling of reduced iron and manganese in the sediments. This promotes re-oxidation of reduced iron and manganese near the sediment surface, and facilitates the downward transport of oxidised species, increasing overall iron and manganese reduction rates (e.g., Jørgensen, 1982; Canfield et al., 1993b). Additionally, Liu et al. (2023) show a complex interplay and influence of OC contents and composition on the formation and types of iron-bearing minerals, which might influence iron reduction rates.

Absolute denitrification rates of all sites in groups 2, 3, 4 and 5 are $0.3 \pm <0.1$ mmol m^{-2} day^{-1}, similar to denitrification rates of 0.4–0.6 mmol m^{-2} day^{-1} reported for fine-grained North Sea sediments in the Skagerrak (Canfield et al., 1993a). As a control on the denitrification rate, Pastor et al. (2011) suggested competition between aerobic respiration and denitrification, while De Borger et al. (2021a) linked the denitrification rate to the nitrate availability. In the HMA, denitrification rates are controlled by the formation of ammonia through OC remineralisation in the sediments, followed by the oxidation of ammonia via nitrification as it diffuses towards the SWI (e.g., Jørgensen, 2021 and references therein). Therefore, in the sediments of the HMA, denitrification rates are directly related to the available OC for degradation in the sediments and thus total OC remineralisation producing ammonia (Fig. 9d). This results in denitrification contributing constantly 6 ± 1 % to total remineralisation for all sites in groups 2, 3, 4 and 5.

As we have shown above, the absolute rates of aerobic and anaerobic processes vary with the benthic OC flux to the sediments of the HMA. However, the relative contributions of aerobic and anaerobic mineralisation pathways are not driven by the magnitude of the benthic OC flux in the HMA. In contrast to our findings in the HMA, a global data compilation of previous publications by Pastor et al. (2011) showed a significant correlation between the logarithmic benthic OC flux and the relative contribution of anaerobic remineralisation to total remineralisation rate ($cor = 0.75$, $p < 0.0001$). However, this compilation spans three orders of magnitude differences in benthic OC fluxes from 1 to 1000 mmol m^{-2} day^{-1}, from deep-sea ecosystems (Soetaert et al., 1996) to salt marshes (Mackin and Swider, 1989), representing various depositional environments. Furthermore, in large areas of the HMA (Fig. 11, groups 2 and 3), the relative contributions of the different metabolic pathways to total OC remineralisation remain constant. This consistency is observed despite sedimentation rates varying by an order of magnitude, mud contents between 53 and 93 %, benthic OC fluxes between 3.6 and 17.8 mmol m^{-2} day^{-1}, and average OC reactivities of 3.1–7.1 yr^{-1}. We conclude that either, (1) sedimentation rate, mud content, benthic OC flux and average OC reactivity do not significantly influence the relative importance of aerobic and anaerobic processes as well as the different pathways of OC remineralisation, or (2) the differences in these parameters are not large enough to create an impact on the contribution of the remineralisation pathways, which would indicate a low sensitivity of the processes to these parameters. Although highly unlikely, all differences in parameters at each station could also promote in combination the same effect on the relative contribution of the individual metabolic pathways. Significant differences in the relative contribution of the anaerobic processes and the different pathways are only observed if the iron and manganese input to the sediments increases (Fig. 12, Table S1) and is not driven by sedimentation rate, mud content, average reactivity of OC, total remineralisation rate or OC supply.

5.5. Areas influenced by anthropogenic activities

The two major anthropogenic activities in the HMA are bottom trawling fisheries and dumping of harbour sediments. Highest bottom trawling activity is reported to occur in the northwestern part of the HMA – including site NW (Hintzen et al., 2012; Thünen Institute, 2018). Here, the average swept area ratio is estimated to be 5 to 15 yr^{-1}, while the rest of the HMA is barely affected by trawling (swept area ratio: 0-2 yr^{-1}; Hintzen et al., 2012; Thünen Institute, 2018). The strong sediment mixing of the surface sediments at site NW is primarily caused by intensive bottom trawling in this area, resulting in ~30 % lower TOC contents compared to nearby sites with similar sedimentation rates (Müller et al., 2025), which is consistent with recent findings for other shelf areas (van de Velde et al., 2018; Paradis et al., 2019; De Borger et al., 2021b; Zhang et al., 2024).

Based on the results of our full diagenetic model at site NW we find that – despite lower average OC contents – total remineralisation rates are similar to those at sites WC and C_{deep} (5.1–5.9 mmol m^{-2} day^{-1}), which are characterised by similar sedimentation rates. Hence, OC remineralisation is relatively high, and preservation efficiency of OC at site NW is low compared to sites with similar sedimentation rates as a consequence of repetitive resuspension and prolonged oxygen exposure time (e.g. Hartnett et al., 1998) of surface sediments induced by bottom trawling fisheries. This finding supports the results of van de Velde et al. (2018) investigating the influence of sediment mixing on biogeochemical processes in the shallow southern North Sea off-shore the Belgian coast. The authors also show enhanced aerobic respiration, iron reduction, manganese reduction and sulphate reduction with an increasing number of disturbances per year. In contrast to the findings on the different pathways of OC remineralisation reported by van de Velde et al. (2018), we find in the HMA at site NW a lower contribution of 48 % aerobic respiration and a significantly higher sulphate reduction rate of 2.1 mmol m^{-2} day^{-1} and contribution of 35.5 % to total OC remineralisation. The sulphate reduction rate at site NW is highest for both absolute sulphate reduction rates and relative contribution to total remineralisation in the entire HMA. This results from the redistribution of reactive OC at site NW due to sediment mixing by bottom trawling (Fig. 11, orange line, Fig. S1). In the HMA most of the degradable fraction of the OC is limited to the uppermost part of the sediment (Fig. 11). Since sediment mixing transports reactive/degradable OC downwards and more refractory OC upwards towards the sediment surface, we find lower rates of aerobic respiration and a larger contribution of sulphate reduction due to the availability of reactive OC at site NW (Fig. 11, orange line; Fig. 12). Additionally, repetitive cycling through oxic and anoxic conditions can promote the overall degradation of OC in surface sediments (e.g., Aller, 1994). Besides the effects of bottom trawling on OC remineralisation, a recent study by Kalapurakkal et al. (2025) shows the strong impact of resuspension by bottom trawling on biogeochemical processes in the water column. The authors show, in addition to the remineralisation of OC in resuspended sediments, that the oxidation of pyrite in the water column impacts the ocean's alkalinity, and ultimately releases large quantities of CO_2 into the atmosphere.

The second significant anthropogenic disturbance in the HMA is the dumping of Hamburg harbour sediments at site Tonne E3 (e.g., Hamburg Port Authority, 2020). Here, we find very low total remineralisation rates of 2.1 mmol m^{-2} day^{-1} and a very high contribution of aerobic respiration to total remineralisation in the order of 83 % (Fig. 12, group 1). Average TOC contents are ~0.6 wt% with the uppermost two cm being lower by ~70 and 50 % (0.2 and 0.3 wt %) compared to the average TOC content of the core. This falls together with a similarly deep oxygen penetration depth of around two cm, leading to enhanced OC remineralisation within the oxic layer.

The OC contents of sediments in various parts of the Hamburg harbour, which are characterised by high sedimentation and consequently frequent sediment management are between 2 and 7.6 wt% (average: 3.8 wt%; Zander et al., 2020). This is 7–12 times higher than the average OC content determined for the samples at site Tonne E3. Compared to the Tonne E3 sediments, incubated sediments from the Elbe river showed higher remineralisation under oxic conditions and one order of magnitude higher OC degradation rates (Zander et al., 2020). Higher OC degradation rates than at Tonne E3 are also found in areas of high OC accumulation and sedimentation, and consequently, sediment management.

As the sediments at the dumping site Tonne E3 consist of coarse sands with low mud content and a mean grain size of 98 μm (Laurer et al., 2013; Wei et al., 2025), we argue that most of the fine-grained and OC-rich material dredged in the Hamburg harbour and dumped at the Tonne E3 site is exported from the dumping site. This is supported by recent findings by Porz et al. (2025) showing the high migration potential of especially the fine-grained fraction of dumped sediments in the southern North Sea, due to the strong hydrodynamical energy levels (Porz et al., 2025). This fine-grained and OC-rich material might undergo repetitive cycles of deposition and resuspension, as well as remineralisation, before final deposition close to the dumping site, the mud flats of the Wadden Sea, within the estuaries or in one of the big depocentres for fine-grained sediments in the North Sea, the Skagerrak and Norwegian Trough (e.g., de Haas et al., 2002; Lenz et al., 2024; Spiegel et al., 2024, 2025; Porz et al., 2025). However, unknown amounts of sediment and hence OC are exported from the dumping site further offshore or towards the coast, eventually deposited elsewhere. This would lead to long oxygen exposure times and enhance OC degradation (e.g., Hartnett et al., 1998), especially since Zander et al. (2020) highlight a three-fold higher OC degradation rate of the harbour sediments under oxic conditions compared to anoxic conditions (see also Kalapurakkal et al., 2025). Consequently, unknown quantities of the OC are ultimately remineralised to CO_2 by dumping harbour sediments into the North Sea, as also suggested by Porz et al. (2025). The importance of future research on sediment dredging and dumping in coastal and marine environments becomes apparent when considering that in the E.U. alone, 200 to 250 million tonnes of sediment are dredged each year, of which ~80 % is dumped in the marine environment (EuDA, 2005), with a high sediment migration and remineralisation potential (Porz et al., 2025).

6. Conclusions

The combination of a comprehensive high-resolution solid-phase and pore-water dataset and the applied full diagenetic model allowed us to quantify the rates and pathways of both aerobic and anaerobic OC degradation in surface sediments of the Helgoland Mud Area (HMA). We successfully corrected the rates of the different metabolic pathways for non-steady state conditions caused by storm-induced pore-water mixing in the shallow-water eastern part of the HMA. The comparison of the results of the full diagenetic model with the empirical approach followed by Müller et al. (2025) showed that the total rates derived from both approaches agree very well. As a consequence, we can thus demonstrate that a robust estimate of total remineralisation rates as well as burial and benthic OC fluxes can be determined with high reliability using solely diffusive oxygen uptake and sedimentation rates.

The integrated total remineralisation rates assessed based on the full diagenetic model are controlled by the availability of labile OC. OC remineralisation below 25 cm accounts for approximately 30 % of the total dissolved inorganic carbon flux across the SWI. Highest organic carbon burial efficiencies of up to 66 % were found in an area stretching from the southern HMA close to the river Elbe outflow towards the north along the slope of the HMA. Here, enhanced degradation of labile compounds under oxic conditions in the water column caused by permanent tidal resuspension and deposition cycles that keep the sediment particles in periodic suspension, resulting in the deposition of lower-reactive OC.

We found that aerobic respiration is the most important and sulphate reduction is the second most important pathway of OC remineralisation within the surface sediments of the HMA. Surprisingly, no effect of the different depositional and geochemical environments was observed neither on the relative contribution of aerobic and anaerobic remineralisation to total remineralisation nor on the relative contribution of the different pathways over a wide range of depositional parameters, including mud contents, sedimentation rates, benthic OC fluxes, and average reactivity of the OC reaching the SWI. These observations indicate that either (1) these parameters do not significantly influence the relative contribution of aerobic and anaerobic processes, as well as the different pathways of OC remineralisation, or (2) the ranges within the individual parameters are too small to generate an effect on the contribution of the remineralisation pathways, indicating a low sensitivity of the processes to these parameters.

In addition to resuspending sediments and enhancing OC remineralisation in the water column, intensive bottom trawling also results in a lower contribution of aerobic respiration to total remineralisation and enhanced sulphate reduction within the sediments. Enhanced sediment mixing transports labile OC from the sediment surface downwards. This downward transport of labile OC potentially promotes overall OC remineralisation and limits the preservation of OC in sediments. The dumping site for harbour sediments Tonne E3 shows a low total OC remineralisation rate and ~7 to 12 times lower TOC contents compared to harbour sediments – at least in the centre of the deposition area. Further investigations are therefore needed to assess the fate of OC during sediment dumping, its impact on benthic and pelagic remineralisation and ultimately CO_2 formation.

CRediT authorship contribution statement

Daniel Müller: Writing – review & editing, Writing – original draft, Visualization, Validation, Investigation, Formal analysis, Data curation, Conceptualization. **Bo Liu:** Writing – review & editing, Software, Formal analysis, Data curation. **Moritz Holtappels:** Writing – review & editing, Funding acquisition, Formal analysis, Conceptualization. **Walter Geibert:** Writing – review & editing. **Susann Henkel:** Writing – review & editing. **Sabine Kasten:** Writing – review & editing, Supervision, Funding acquisition, Conceptualization.

Financial support

This work was carried out as part of the project “Anthropogenic impacts on particulate organic carbon cycling in the North Sea” (APOC) funded by the German Federal Ministry of Education and Research (BMBF) (03F0874A) in the framework of the MARE:N “The Oceans under Stress” programme. Additional financial support was provided by the Helmholtz Association (Alfred Wegener Institute Helmholtz Centre for Polar and Marine Research) in the framework of the Helmholtz Research Program “Changing Earth – Sustaining our Future” in PoF IV and Germany's Excellence Strategy Cluster of Excellence EXC-2077-390741603.

Declaration of competing interest

The authors declare that they have no known competing financial interests or personal relationships that could have appeared to influence the work reported in this paper.

Acknowledgements

We thank the captains, crew and scientific teams on board RV Heincke cruise HE595 (Grant Number: HE-595) for their technical and scientific support. Thanks to Fabrizio Minutolo (Hereon) for the support

in on-board sampling. For analytical support on board and in the home laboratory, we thank Ingrid Dohrmann and Denise Bethke (both AWI). We also thank Xiting Liu and the anonymous reviewer for their helpful and constructive feedback on the manuscript, and editor Gary Fones for the assistance.

Appendix A. Supplementary data

Supplementary data to this article can be found online at https://doi.org/10.1016/j.csr.2025.105632.

Data availability

The data presented in this study is available via the PANGAEA repository (https://doi.org/10.1594/PANGAEA.983806; https://doi.org/10.1594/PANGAEA.983802).

References

Abromeit, C., Bold, S., Hunke, A., Brauch, J., Mansfeld, M., Rossbach, L., Thoma, D., Trümpler, K., Schröder-Fürstenberg, J., Weigelt, A., Wunsch, M., Zabrocki, M., Fischer, J.-G., Westfeld, P., 2022. Für Meer Und Mensch, Schifffahrt Und Umwelt Jahresbericht 2022. Rostock.

Aller, R.C., 1994. Bioturbation and remineralization of sedimentary organic matter: effects of redox oscillation. Chem. Geol. 114, 331–345. https://doi.org/10.1016/0009-2541(94)90062-0.

Aller, R.C., Madrid, V., Chistoserdov, A., Aller, J.Y., Heilbrun, C., 2010. Unsteady diagenetic processes and sulfur biogeochemistry in tropical deltaic muds: implications for Oceanic isotope cycles and the sedimentary record. Geochem. Cosmochim. Acta 74, 4671–4692. https://doi.org/10.1016/j.gca.2010.05.008.

Anggara Kasih, G.A., Chiba, S., Yamagata, Y., Shimizu, Y., Haraguchi, K., 2009. Numerical model on the material circulation for coastal sediment in Ago Bay, Japan. J. Mar. Syst. 77, 45–60. https://doi.org/10.1016/j.jmarsys.2008.11.006.

Arndt, S., Jørgensen, B.B., LaRowe, D.E., Middelburg, J.J., Pancost, R.D., Regnier, P., 2013. Quantifying the degradation of organic matter in marine sediments: a review and synthesis. Earth Sci. Rev. 123, 53–86. https://doi.org/10.1016/j.earscirev.2013.02.008.

Baloza, M., Henkel, S., Geibert, W., Kasten, S., Holtappels, M., 2022. Benthic carbon remineralization and iron cycling in relation to sea ice cover along the eastern continental shelf of the Antarctic Peninsula. J. Geophys. Res. Ocean. 127. https://doi.org/10.1029/2021JC018401.

Berg, P., Rysgaard, S., Thamdrup, B., 2003. Dynamic modeling of early diagenesis and nutrient cycling. A case study in an arctic marine sediment. Am. J. Sci. 303, 905–955. https://doi.org/10.2475/ajs.303.10.905.

Berner, R.A., 1982. Burial of organic carbon and pyrite sulfur in the modern ocean: its geochemical and environmental significance. Am. J. Sci. 282, 451–473. https://doi.org/10.2475/ajs.282.4.451.

Berner, R.A., 1980. Early Diagenesis: a Theoretical Approach. Princeton University Press.

Bockelmann, F.-D., Puls, W., Kleeberg, U., Müller, D., Emeis, K.-C., 2018. Mapping mud content and median grain-size of North Sea sediments – a geostatistical approach. Mar. Geol. 397, 60–71. https://doi.org/10.1016/j.margeo.2017.11.003.

Boudreau, B.P., 1997. Diagenetic Models and their Implementation. Springer Berlin Heidelberg, Berlin, Heidelberg. https://doi.org/10.1007/978-3-642-60421-8.

Boudreau, B.P., 1996a. A method-of-lines code for carbon and nutrient diagenesis in aquatic sediments. Comput. Geosci. 22, 479–496. https://doi.org/10.1016/0098-3004(95)00115-8.

Boudreau, B.P., 1996b. The diffusive tortuosity of fine-grained unlithified sediments. Geochem. Cosmochim. Acta 60, 3139–3142. https://doi.org/10.1016/0016-7037(96)00158-5.

Bowles, M.W., Mogollon, J.M., Kasten, S., Zabel, M., Hinrichs, K.-U., 2014. Global rates of marine sulfate reduction and implications for sub-sea-floor metabolic activities. Science 344, 889–891. https://doi.org/10.1126/science.1249213.

Boyle, E.A., Edmond, J.M., Sholkovitz, E.R., 1977. The mechanism of iron removal in estuaries. Geochem. Cosmochim. Acta 41, 1313–1324. https://doi.org/10.1016/0016-7037(77)90075-8.

Burdige, D., Skoog, A., Gardner, K., 2000. Dissolved and particulate carbohydrates in contrasting marine sediments. Geochem. Cosmochim. Acta 64, 1029–1041. https://doi.org/10.1016/S0016-7037(99)00361-0.

Burdige, D.J., 2007. Preservation of organic matter in marine sediments: controls, mechanisms, and an imbalance in sediment organic carbon budgets? Chem. Rev. 107, 467–485. https://doi.org/10.1021/cr050347q.

Burdige, D.J., 2006. Geochemistry of Marine Sediments. Princeton University Press, Princeton.

Canfield, D.E., 1994. Factors influencing organic carbon preservation in marine sediments. Chem. Geol. 114, 315–329. https://doi.org/10.1016/0009-2541(94)90061-2.

Canfield, D.E., 1989. Sulfate reduction and oxic respiration in marine sediments: implications for organic carbon preservation in euxinic environments. Deep-Sea Res., Part A 36, 121–138. https://doi.org/10.1016/0198-0149(89)90022-8.

Canfield, D.E., Jørgensen, B.B., Fossing, H., Glud, R., Gundersen, J., Ramsing, N.B., Thamdrup, B., Hansen, J.W., Nielsen, L.P., Hall, P.O.J., 1993a. Pathways of organic carbon oxidation in three continental margin sediments. Mar. Geol. 113, 27–40. https://doi.org/10.1016/0025-3227(93)90147-N.

Canfield, D.E., Thamdrup, B., Hansen, J.W., 1993b. The anaerobic degradation of organic matter in Danish coastal sediments: iron reduction, manganese reduction, and sulfate reduction. Geochem. Cosmochim. Acta 57, 3867–3883. https://doi.org/10.1016/0016-7037(93)90340-3.

Chen, J., Zhang, W., Porz, L., Arlinghaus, P., Hanz, U., Holtappels, M., Schrum, C., 2025. Physical mechanisms of sediment trapping and deposition on spatially confined mud depocenters in high-energy Shelf Seas. J. Geophys. Res. Ocean. 130. https://doi.org/10.1029/2025JC022622.

Christensen, J.P., 1989. Sulfate reduction and carbon oxidation rates in continental shelf sediments, an examination of offshelf carbon transport. Cont. Shelf Res. 9, 223–246. https://doi.org/10.1016/0278-4343(89)90025-3.

Clare, M.A., Lichtschlag, A., Paradis, S., Barlow, N.L.M., 2023. Assessing the impact of the global subsea telecommunications network on sedimentary organic carbon stocks. Nat. Commun. 14, 2080. https://doi.org/10.1038/s41467-023-37854-6.

Cline, J.D., 1969. Spectrophotometric determination of hydrogen sulfide in natural waters. Limnol. Oceanogr. 14, 454–458. https://doi.org/10.4319/lo.1969.14.3.0454.

De Borger, E., Braeckman, U., Soetaert, K., 2021a. Rapid organic matter cycling in North Sea sediments. Cont. Shelf Res. 214, 104327. https://doi.org/10.1016/j.csr.2020.104327.

De Borger, E., Tiano, J., Braeckman, U., Rijnsdorp, A.D., Soetaert, K., 2021b. Impact of bottom trawling on sediment biogeochemistry: a modelling approach. Biogeosciences 18, 2539–2557. https://doi.org/10.5194/bg-18-2539-2021.

de Groot, S.J., 1984. The impact of bottom trawling on benthic fauna of the North Sea. Ocean Manag. 9, 177–190. https://doi.org/10.1016/0302-184X(84)90002-7.

de Haas, H., Okkels, E., van Weering, T.C.E., 1996. Recent sediment accumulation in the Norwegian Channel, North Sea. NGU-Bulletin 430, 57–65.

de Haas, H., van Weering, T.C.E., de Stigter, H., 2002. Organic carbon in shelf seas: sinks or sources, processes and products. Cont. Shelf Res. 22, 691–717. https://doi.org/10.1016/S0278-4343(01)00093-0.

Doll, M.K.M., 2015. Reflexionsseismische Und Hydroakustische Untersuchungen Des Helgoländer Schlickgebietes in Der Südlichen Nordsee. B.S. Thesis. University of Bremen.

Eigaard, O.R., Bastardie, F., Hintzen, N.T., Buhl-Mortensen, L., Buhl-Mortensen, P., Catarino, R., Dinesen, G.E., Egekvist, J., Fock, H.O., Geitner, K., Gerritsen, H.D., González, M.M., Jonsson, P., Kavadas, S., Laffargue, P., Lundy, M., Gonzalez-Mirelis, G., Nielsen, J.R., Papadopoulou, N., Posen, P.E., Pulcinella, J., Russo, T., Sala, A., Silva, C., Smith, C.J., Vanelslander, B., Rijnsdorp, A.D., 2017. The footprint of bottom trawling in European waters: distribution, intensity, and seabed integrity. ICES J. Mar. Sci. 74, 847–865. https://doi.org/10.1093/icesjms/fsw194.

Epping, E., van der Zee, C., Soetaert, K., Helder, W., 2002. On the oxidation and burial of organic carbon in sediments of the Iberian margin and Nazaré Canyon (NE Atlantic). Prog. Oceanogr. 52, 399–431. https://doi.org/10.1016/S0079-6611(02)00017-4.

EuDA, 2005. Dredging Makes Sense - Euda Annual Report 2005.

Figge, K., 1981. Sedimentverteilung in Der Deutschen Bucht, Deutsches Hydrographisches Institut, Karte Nr. 2900 (mit Begleitheft).

Fischer, D., Sahling, H., Nöthen, K., Bohrmann, G., Zabel, M., Kasten, S., 2012. Interaction between hydrocarbon seepage, chemosynthetic communities, and bottom water redox at cold seeps of the Makran accretionary prism: insights from habitat-specific pore water sampling and modeling. Biogeosciences 9, 2013–2031. https://doi.org/10.5194/bg-9-2013-2012.

Freitas, F.S., Pika, P.A., Kasten, S., Jørgensen, B.B., Rassmann, J., Rabouille, C., Thomas, S., Sass, H., Pancost, R.D., Arndt, S., 2021. New insights into large-scale trends of apparent organic matter reactivity in marine sediments and patterns of benthic carbon transformation. Biogeosciences 18, 4651–4679. https://doi.org/10.5194/bg-18-4651-2021.

Froelich, P.N., Klinkhammer, G.P., Bender, M.L., Luedtke, N.A., Heath, G.R., Cullen, D., Dauphin, P., Hammond, D., Hartman, B., Maynard, V., 1979. Early oxidation of organic matter in pelagic sediments of the eastern equatorial Atlantic: suboxic diagenesis. Geochem. Cosmochim. Acta 43, 1075–1090. https://doi.org/10.1016/0016-7037(79)90095-4.

Gadow, S., 1969. Gips als Leitmineral für das Liefergebiet Helgoland und für den Transport bei Sturmfluten. Nat. Mus. 99, 537–540.

Glud, R.N., 2008. Oxygen dynamics of marine sediments. Mar. Biol. Res. 4, 243–289. https://doi.org/10.1080/17451000801888726.

Grant, J., Hatcher, A., Macpherson, P., Schofield, B., 1998. Sulfate reduction and total benthic metabolism in shelf and slope sediments off Nova Scotia. Vie Milieu 48, 259–269.

Haeckel, M., Boudreau, B.P., Wallmann, K., 2007. Bubble-induced porewater mixing: a 3-D model for deep porewater irrigation. Geochem. Cosmochim. Acta 71, 5135–5154. https://doi.org/10.1016/j.gca.2007.08.011.

Hamburg Port Authority, 2024. Umgang Mit Baggergut Aus Dem Hamburger Hafen Teilbericht Verbringung Von Baggergut Zur Tonne E3 - Bericht Über Den Zeitraum 1.1.2021 Bis 31.12.2022.

Hamburg Port Authority, 2020. Verbringung Von Hamburger Baggergut in Die Nordsee (Tonne E3).

Hamburg Port Authority, 2017. Umgang Mit Baggergut Aus Dem Hamburger Hafen Verbringung Von Baggergut Zur Tonne E3.

Hanz, U., Wei, B., Müller, D., Fovonova, V., Sander, L., Kopte, R., Kasten, S., Holtappels, M., in preparation. The Influence of Hydrodynamics on the Carbon Burial Efficiency of a Shallow Shelf Carbon Depocenter.

Hartnett, H.E., Keil, R.G., Hedges, J.I., Devol, A.H., 1998. Influence of oxygen exposure time on organic carbon preservation in continental margin sediments. Nature 391, 572–575. https://doi.org/10.1038/35351.
Hedges, J.I., Keil, R.G., 1995. Sedimentary organic matter preservation: an assessment and speculative synthesis. Mar. Chem. 49, 81–115. https://doi.org/10.1016/0304-4203(95)00008-F.
Heinatz, K., Scheffold, M.I.E., 2023. A first estimate of the effect of offshore wind farms on sedimentary organic carbon stocks in the Southern North Sea. Front. Mar. Sci. 9, 1–8. https://doi.org/10.3389/fmars.2022.1068967.
Henkel, S., Kasten, S., Poulton, S.W., Staubwasser, M., 2016. Determination of the stable iron isotopic composition of sequentially leached iron phases in marine sediments. Chem. Geol. 421, 93–102. https://doi.org/10.1016/j.chemgeo.2015.12.003.
Henkel, S., Liu, B., Staubwasser, M., Kasemann, S.A., Meixner, A., Aromokeye, D.A., Friedrich, M.W., Kasten, S., 2025. Stable iron isotope signals indicate a "pseudo-abiotic" process driving deep iron release in methanic sediments. Biogeosciences 22, 1673–1696. https://doi.org/10.5194/bg-22-1673-2025.
Henkel, S., Schwenk, T., Hanebuth, T.J.J., Strasser, M., Riedinger, N., Formolo, M., Tomasini, J., Krastel, S., 2012. Pore water geochemistry as a tool for identifying and dating recent mass-transport deposits. In: Yamada, Y., Kawamura, K., Ikehara, K., Ogawa, Y., Urgeles, R., Mosher, D., Chaytor, J., Strasser, M. (Eds.), Submarine Mass Movements and Their Consequences. Springer, Netherlands, Dordrecht. https://doi.org/10.1007/978-94-007-2162-3.
Henrichs, S.M., Reeburgh, W.S., 1987. Anaerobic mineralization of marine sediment organic matter: rates and the role of anaerobic processes in the oceanic carbon economy. Geomicrobiol. J. 5, 191–237. https://doi.org/10.1080/01490458709385971.
Hensen, C., Zabel, M., Pfeifer, K., Schwenk, T., Kasten, S., Riedinger, N., Schulz, H.D., Boetius, A., 2003. Control of sulfate pore-water profiles by sedimentary events and the significance of anaerobic oxidation of methane for the burial of sulfur in marine sediments. Geochem. Cosmochim. Acta 67, 2631–2647. https://doi.org/10.1016/S0016-7037(03)00199-6.
Hintzen, N.T., Bastardie, F., Beare, D., Piet, G.J., Ulrich, C., Deporte, N., Egekvist, J., Degel, H., 2012. VMStools: Open-source software for the processing, analysis and visualisation of fisheries logbook and VMS data. Fish. Res. 115–116, 31–43. https://doi.org/10.1016/j.fishres.2011.11.007.
Hertweck, G., 1983. Das Schlickgebiet in der inneren Deutschen Bucht. Senckenberg. Maritima 15, 219–249.
Jørgensen, B.B., 2021. Sulfur biogeochemical cycle of marine sediments. Geochemical Perspect 10, 1–174. https://doi.org/10.7185/geochempersp.10.2.
Jørgensen, B.B., 1982. Mineralization of organic matter in the sea bed—the role of sulphate reduction. Nature 296, 643–645. https://doi.org/10.1038/296643a0.
Jørgensen, B.B., 1978. A comparison of methods for the quantification of bacterial sulfate reduction in coastal marine sediments. Geomicrobiol. J. 1, 11–27. https://doi.org/10.1080/01490457809377721.
Jørgensen, B., Bang, M., Blackburn, T., 1990. Anaerobic mineralization in marine sediments from the Baltic Sea-North Sea transition. Mar. Ecol. Prog. Ser. 59, 39–54. https://doi.org/10.3354/meps059039.
Jørgensen, B.B., Kasten, S., 2006. Sulfur cycling and methane oxidation. In: Marine Geochemistry. Springer-Verlag, Berlin/Heidelberg, pp. 271–309. https://doi.org/10.1007/3-540-32144-6_8.
Jung, M., Ilmberger, J., Mangini, A., Emeis, K.-C., 1997. Why some Mediterranean sapropels survived burn-down (and others did not). Mar. Geol. 141, 51–60. https://doi.org/10.1016/S0025-3227(97)00031-5.
Kalapurakkal, H.T., Dale, A.W., Schmidt, M., Taubner, H., Scholz, F., Spiegel, T., Fuhr, M., Wallmann, K., 2025. Sediment resuspension in muddy sediments enhances pyrite oxidation and carbon dioxide emissions in Kiel Bight. Commun. Earth Environ. 6, 156. https://doi.org/10.1038/s43247-025-02132-4.
Kasten, S., Zabel, M., Heuer, V., Hensen, C., 2003. Processes and signals of nonsteady-state diagenesis in deep-sea sediments and their pore waters. In: The South Atlantic in the Late Quaternary. Springer Berlin Heidelberg, Berlin, Heidelberg, pp. 431–459. https://doi.org/10.1007/978-3-642-18917-3_20.
Kristensen, E., Devol, A.H., Hartnett, H.E., 1999. Organic matter diagenesis in sediments on the continental shelf and slope of the Eastern Tropical and temperate North Pacific. Cont. Shelf Res. 19, 1331–1351. https://doi.org/10.1016/S0278-4343(99)00024-2.
Laurer, W.-U., Naumann, M., Zeiler, M., 2013. Erstellung Der Karte Zur Sedimentverteilung Auf Dem Meeresboden in Der Deutschen Nordsee Nach Der Klassifikation Von FIGGE (1981).
Lee, T.R., Wood, W.T., Phrampus, B.J., 2019. A machine learning (kNN) approach to predicting global seafloor total organic carbon. Glob. Biogeochem. Cycles 33, 37–46. https://doi.org/10.1029/2018GB005992.
Lenz, N., Spiegel, T., Hathorne, E., Wallmann, K., Eisenhauer, A., Frank, M., 2024. Provenance of clay-sized detrital sediments in the North Sea and the Skagerrak region based on radiogenic nd-sr-hf isotopes and clay mineral compositions: assessing the impact of coastal and seabed erosion. Front. Mar. Sci. 11. https://doi.org/10.3389/fmars.2024.1416519.
Lipka, M., Woelfel, J., Gogina, M., Kallmeyer, J., Liu, B., Morys, C., Forster, S., Böttcher, M.E., 2018. Solute reservoirs reflect variability of early diagenetic processes in temperate brackish surface sediments. Front. Mar. Sci. 5, 1–20. https://doi.org/10.3389/fmars.2018.00413.
Liu, B., Müller, D., Henkel, S., Geneste, C., Holtappels, M., Kasten, S., in preparation. Carbon diagenesis and long-term burial as carbonate in sediments of the Helgoland Mud Area, SE German Bight.
Liu, X., Gu, Y., Dong, J., Li, A., Zhuang, G., Wang, H., 2023. Iron-bearing minerals indicate sea-level rise of the East China Sea inner shelf since the last deglaciation. Sci. Bull. 68, 364–366. https://doi.org/10.1016/j.scib.2023.02.002.
Mackin, J.E., Swider, K.T., 1989. Organic matter decomposition pathways and oxygen consumption in coastal marine sediments. J. Mar. Res. 47, 681–716.
Meister, P., Liu, B., Khalili, A., Böttcher, M.E., Jørgensen, B.B., 2019. Factors controlling the carbon isotope composition of dissolved inorganic carbon and methane in marine porewater: an evaluation by reaction-transport modelling. J. Mar. Syst. 200, 103227. https://doi.org/10.1016/j.jmarsys.2019.103227.
Middelburg, J.J., 2018. Reviews and syntheses: to the bottom of carbon processing at the seafloor. Biogeosciences 15, 413–427. https://doi.org/10.5194/bg-15-413-2018.
Middelburg, J.J., Soetaert, K., Herman, P.M.J., 1997. Empirical relationships for use in global diagenetic models. Deep-Sea Res. Part I Oceanogr. Res. Pap. 44, 327–344. https://doi.org/10.1016/S0967-0637(96)00101-X.
Middelburg, J.J., Vlug, T., Jaco, F., van der Nat, W.A., 1993. Organic matter mineralization in marine systems. Global Planet. Change 8, 47–58. https://doi.org/10.1016/0921-8181(93)90062-S.
Mogollón, J.M., Mewes, K., Kasten, S., 2016. Quantifying manganese and nitrogen cycle coupling in manganese-rich, organic carbon-starved marine sediments: examples from the Clarion-Clipperton fracture zone. Geophys. Res. Lett. 43, 7114–7123. https://doi.org/10.1002/2016GL069117.
Müller, D., Liu, B., Geibert, W., Holtappels, M., Sander, L., Miramontes, E., Taubner, H., Henkel, S., Hinrichs, K.-U., Bethke, D., Dohrmann, I., Kasten, S., 2025. Depositional controls and budget of organic carbon burial in fine-grained sediments of the North Sea – the Helgoland Mud Area as a natural laboratory. Biogeosciences 22, 2541–2567. https://doi.org/10.5194/bg-22-2541-2025.
Oni, O., Miyatake, T., Kasten, S., Richter-Heitmann, T., Fischer, D., Wagenknecht, L., Kulkarni, A., Blumers, M., Shylin, S.I., Ksenofontov, V., Costa, B.F.O., Klingelhöfer, G., Friedrich, M.W., 2015. Distinct microbial populations are tightly linked to the profile of dissolved iron in the methanic sediments of the Helgoland mud area, North Sea. Front. Microbiol. 6, 1–15. https://doi.org/10.3389/fmicb.2015.00365.
Paradis, S., Goñi, M., Masqué, P., Durán, R., Arjona-Camas, M., Palanques, A., Puig, P., 2021. Persistence of biogeochemical alterations of deep-sea sediments by bottom trawling. Geophys. Res. Lett. 48, 1–12. https://doi.org/10.1029/2020GL091279.
Paradis, S., Pusceddu, A., Masqué, P., Puig, P., Moccia, D., Russo, T., Lo Iacono, C., 2019. Organic matter contents and degradation in a highly trawled area during fresh particle inputs (Gulf of Castellammare, southwestern Mediterranean). Biogeosciences 16, 4307–4320. https://doi.org/10.5194/bg-16-4307-2019.
Pastor, L., Cathalot, C., Deflandre, B., Viollier, E., Soetaert, K., Meysman, F.J.R., Ulses, C., Metzger, E., Rabouille, C., 2011. Modeling biogeochemical processes in sediments from the Rhône River prodelta area (NW Mediterranean Sea). Biogeosciences 8, 1351–1366. https://doi.org/10.5194/bg-8-1351-2011.
Porz, L., Chen, J., Yilmaz, R., Kuhlmann, J., Zhang, W., Schrum, C., 2025. Dredging and dumping impact coastal fluxes of sediment and organic carbon [preprint]. Res. Sq. https://doi.org/10.21203/rs.3.rs-6005877/v1.
Puls, W., Beusekom, J., Brockmann, U., Doerffer, R., Hentschke, U., König, P., Murphy, D., Mayer, B., Müller, A., Pohlmann, T., Reimer, A., Schmidt-Nia, R., Sündermann, J., 1999. SPM concentrations in the German Bight: comparison between a model simulation and measurements. Dtsch. Hydrogr. Zeitschrift 51, 221–244. https://doi.org/10.1007/BF02764175.
Ren, J.-H., Zhu, M.-X., Wang, D.-Y., Tan, T.-T., Li, T., Zhao, M., Pan, D.-W., 2022. Organic carbon mineralization pathways in the muddy sediments of the South Yellow Sea: insights from steady-state modeling of porewater. Appl. Geochem. 138, 105237. https://doi.org/10.1016/j.apgeochem.2022.105237.
Riedinger, N., Brunner, B., Krastel, S., Arnold, G.L., Wehrmann, L.M., Formolo, M.J., Beck, A., Bates, S.M., Henkel, S., Kasten, S., Lyons, T.W., 2017. Sulfur cycling in an iron Oxide-Dominated, dynamic marine depositional System: the Argentine Continental Margin. Front. Earth Sci. 5. https://doi.org/10.3389/feart.2017.00033.
Santos, I.R., Eyre, B.D., Huettel, M., 2012. The driving forces of porewater and groundwater flow in permeable coastal sediments: a review. Estuar. Coast Shelf Sci. 98, 1–15. https://doi.org/10.1016/j.ecss.2011.10.024.
Seeberg-Elverfeldt, J., Schlüter, M., Feseker, T., Kölling, M., 2005. Rhizon sampling of porewaters near the sediment-water interface of aquatic systems. Limnol Oceanogr. Methods 3, 361–371. https://doi.org/10.4319/lom.2005.3.361.
Sievers, J., Milbradt, P., Ihde, R., Valerius, J., Hagen, R., Plüß, A., 2021. An integrated marine data collection for the German Bight – part 1: subaqueous geomorphology and surface sedimentology (1996–2016). Earth Syst. Sci. Data 13, 4053–4065. https://doi.org/10.5194/essd-13-4053-2021.
Soetaert, K., Herman, P.M.J., Middelburg, J.J., 1996. Dynamic response of deep-sea sediments to seasonal variations: a model. Limnol. Oceanogr. 41, 1651–1668. https://doi.org/10.4319/lo.1996.41.8.1651.
Soetaert, K., Meysman, F., 2012. Reactive transport in aquatic ecosystems: rapid model prototyping in the open source software R. Environ. Model. Software 32, 49–60. https://doi.org/10.1016/j.envsoft.2011.08.011.
Soetaert, K., Petzoldt, T., Meysman, F., 2010. Marelac: Tools for Aquatic Sciences. R Packag version 2.1.
Spiegel, T., Diesing, M., Dale, A.W., Lenz, N., Schmidt, M., Sommer, S., Böttner, C., Fuhr, M., Kalapurakkal, H.T., Schulze, C.-S., Wallmann, K., 2024. Modelling mass accumulation rates and 210Pb rain rates in the Skagerrak: lateral sediment transport dominates the sediment input. Front. Mar. Sci. 11, 1–14. https://doi.org/10.3389/fmars.2024.1331102.
Spiegel, T., Dale, A.W., Lenz, N., Schmidt, M., Moros, M., Lindhorst, S., Wolschke, H., Müller, D., Butzin, M., Fuhr, M., Kalapurakkal, H.T., Kasten, S., Wallmann, K., 2025. Mass accumulation rates decreased in the Skagerrak basin over the last 100 years. Cont. Shelf Res. 286, 105411. https://doi.org/10.1016/j.csr.2025.105411.
Ståhl, H., Tengberg, A., Brunnegård, J., Bjørnbom, E., Forbes, T.L., Josefson, A.B., Kaberi, H.G., Hassellöv, I.M.K., Olsgard, F., Roos, P., Hall, P.O.J., 2004. Factors

influencing organic carbon recycling and burial in Skagerrak sediments. J. Mar. Res. 62, 867–907. https://doi.org/10.1357/0022240042880873.
Suess, E., 1980. Particulate organic carbon flux in the oceans—surface productivity and oxygen utilization. Nature 288, 260–263. https://doi.org/10.1038/288260a0.
Thamdrup, B., Canfield, D.E., 1996. Pathways of carbon oxidation in continental margin sediments off central Chile. Limnol. Oceanogr. 41, 1629–1650. https://doi.org/10.4319/lo.1996.41.8.1629.
Thünen Institute, 2018. Fine-Scale Footprint of Bottom Trawling in the German EEZ of the North Sea, pp. 2012–2016.
Van Cappellen, P., Wang, Y., 1996. Cycling of iron and manganese in surface sediments: a general theory for the coupled transport and reaction of carbon, oxygen, nitrogen, sulfur, iron, and manganese. Am. J. Sci. 296, 197–243. https://doi.org/10.2475/ajs.296.3.197.
van de Velde, S., Van Lancker, V., Hidalgo-Martinez, S., Berelson, W.M., Meysman, F.J. R., 2018. Anthropogenic disturbance keeps the coastal seafloor biogeochemistry in a transient state. Sci. Rep. 8, 5582. https://doi.org/10.1038/s41598-018-23925-y.
Vink, A., Steffen, H., Reinhardt, L., Kaufmann, G., 2007. Holocene relative sea-level change, isostatic subsidence and the radial viscosity structure of the mantle of northwest Europe (Belgium, the Netherlands, Germany, southern North Sea). Quat. Sci. Rev. 26, 3249–3275. https://doi.org/10.1016/j.quascirev.2007.07.014.
Volz, J.B., Liu, B., Köster, M., Henkel, S., Koschinsky, A., Kasten, S., 2020. Post-depositional manganese mobilization during the last glacial period in sediments of the eastern Clarion-Clipperton Zone, Pacific Ocean. Earth Planet Sci. Lett. 532, 116012. https://doi.org/10.1016/j.epsl.2019.116012.
von Haugwitz, W., Wong, H.K., Salge, U., 1988. The mud area southeast of Helgoland: a reflection seismic study. Mitteilungen aus dem Geol. Inst. der Univ. Hambg. 65, 409–422.
Wei, B., Müller, D., Kusch, S., Niu, L., Hefter, J., Sander, L., Hanz, U., Mollenhauer, G., Jia, G., Kasten, S., Holtappels, M., 2025. Twice the global average carbon burial efficiency in the Helgoland Mud Area of the North Sea: insights into carbon sequestration in small-size depocenters on sand-dominated shelves. Chem. Geol. 681, 122712. https://doi.org/10.1016/j.chemgeo.2025.122712.
Xu, S., Liu, B., Arndt, S., Kasten, S., Wu, Z., 2023. Assessing global-scale organic matter reactivity patterns in marine sediments using a lognormal reactive continuum model. Biogeosciences 20, 2251–2263. https://doi.org/10.5194/bg-20-2251-2023.
Zander, F., Heimovaara, T., Gebert, J., 2020. Spatial variability of organic matter degradability in tidal Elbe sediments. J. Soils Sediments 20, 2573–2587. https://doi.org/10.1007/s11368-020-02569-4.
Zeiler, M., Schulz-Ohlberg, J., Figge, K., 2000. Mobile sand deposits and shoreface sediment dynamics in the inner German Bight (North Sea). Mar. Geol. 170, 363–380. https://doi.org/10.1016/S0025-3227(00)00089-X.
Zhang, W., Porz, L., Yilmaz, R., Wallmann, K., Spiegel, T., Neumann, A., Holtappels, M., Kasten, S., Kuhlmann, J., Ziebarth, N., Taylor, B., Ho-Hagemann, H.T.M., Bockelmann, F.-D., Daewel, U., Bernhardt, L., Schrum, C., 2024. Long-term carbon storage in shelf sea sediments reduced by intensive bottom trawling. Nat. Geosci. 17, 1268–1276. https://doi.org/10.1038/s41561-024-01581-4.
Zhou, Z., Henkel, S., Kasten, S., Holtappels, M., 2023. The iron “redox battery” in sandy sediments: its impact on organic matter remineralization and phosphorus cycling. Sci. Total Environ. 865, 161168. https://doi.org/10.1016/j.scitotenv.2022.161168.
Zonneveld, K.A.F., Versteegh, G.J.M., Kasten, S., Eglinton, T.I., Emeis, K.-C., Huguet, C., Koch, B.P., de Lange, G.J., de Leeuw, J.W., Middelburg, J.J., Mollenhauer, G., Prahl, F.G., Rethemeyer, J., Wakeham, S.G., 2010. Selective preservation of organic matter in marine environments; processes and impact on the sedimentary record. Biogeosciences 7, 483–511. https://doi.org/10.5194/bg-7-483-2010.